CHARACTERIZATION OF REDUCED GRAPHENE OXIDE ANODE FOR APPLICATION IN ALGAE BIOPHOTOVOLTAIC PLATFORMS

SITI AISYAH BINTI IBRAHIM

FACULTY OF SCIENCE
UNIVERSITI MALAYA
KUALA LUMPUR

2020

CHARACTERIZATION OF REDUCED GRAPHENE OXIDE ANODE FOR APPLICATION IN ALGAE BIOPHOTOVOLTAIC PLATFORMS

SITI AISYAH BINTI IBRAHIM

DISSERTATION SUBMITTED IN FULFILMENT OF THE REQUIREMENTS FOR THE DEGREE OF MASTER OF SCIENCE

DEPARTMENT OF PHYSICS
FACULTY OF SCIENCE
UNIVERSITI MALAYA
KUALA LUMPUR

2020

UNIVERSITI MALAYA

ORIGINAL LITERARY WORK DECLARATION

Name of Candidate: **SITI AISYAH BINTI IBRAHIM**

Matric No: **SGR140049**

Name of Degree: **MASTER OF SCIENCE**

Title of Project Thesis: **CHARACTERIZATION OF REDUCED GRAPHENE OXIDE A NODE FOR APPLICATION IN ALGAE BIOPHOTOVOLTAIC PLATFORMS**

Field of Study: **EXPERIMENTAL PHYSICS**

I do solemnly and sincerely declare that:

(1) I am the sole author/writer of this Work;
(2) This Work is original;
(3) Any use of any work in which copyright exists was done by way of fair dealing and for permitted purposes and any excerpt or extract from, or reference to or reproduction of any copyright work has been disclosed expressly and sufficiently and the title of the Work and its authorship have been acknowledged in this Work;
(4) I do not have any actual knowledge nor do I ought reasonably to know that the making of this work constitutes an infringement of any copyright work;
(5) I hereby assign all and every rights in the copyright to this Work to the Universiti Malaya ("UM"), who henceforth shall be owner of the copyright in this Work and that any reproduction or use in any form or by any means whatsoever is prohibited without the written consent of UM having been first had and obtained;
(6) I am fully aware that if in the course of making this Work I have infringed any copyright whether intentionally or otherwise, I may be subject to legal action or any other action as may be determined by UM.

Candidate's Signature Date:

Subscribed and solemnly declared before,

Witness's Signature Date:

Name:

Designation:

CHARACTERIZATION OF REDUCED GRAPHENE OXIDE ANODE FOR APPLICATION IN ALGAE BIOPHOTOVOLTAIC PLATFORMS

ABSTRACT

Research interest in recent times has placed much focus on electrode technology for biophotovoltaics (BPV) especially in algal fuel cells (AFCs) application. The purpose of this investigation is therefore directed towards optimizing reduced graphene oxide (rGO) thin film as an electrode for AFCs application by means of annealing and plasma treatment. First stage involves deposition of six (6) layers of rGO thin film using Langmuir-Blodgett (LB) method. The anode electrodes were then annealed at different temperatures under vacuum condition. For plasma treatment meanwhile, a variation of voltage was used to vary the plasma conditions resulting in different surface morphology. To characterize the multilayer films fabricated, the thin films were characterized by means of spectroscopic, structural and electrical studies. In general, results indicate improvement in conductivity and wettability test, which may prove beneficial for implementation in AFCs, and promote improved algae growth, adhesion and photosynthesis yield as an outcome of higher charge mobility.

Keywords: Reduced Graphene Oxide, Langmuir-Blodgett, Biophotovoltaic, Plasma Treatment, Annealing Treatment.

PENCIRIAN ANOD GRAFIN OKSIDA YANG DITURUNKAN SEBAGAI PLATFORM DALAM APLIKASI ALGA BIOFOTOVOLTIK

ABSTRAK

Kepentingan penyelidikan kebelakangan ini telah meletakkan tumpuan pada teknologi elektrod untuk aplikasi biophotovoltik (BPV) terutamanya dalam sel-sel bahan bakar yang berasaskan algal (AFCs). Oleh itu, tujuan siasatan ini dihalakan ke arah mengoptimumkan filem nipis grafin oksida yang diturunkan (rGO) sebagai elektrod untuk aplikasi AFCs dengan kaedah sepuh lindap dan plasma. Peringkat pertama melibatkan pemendapan enam lapisan filem nipis rGO dengan menggunakan kaedah Langmuir-Blodgett (LB). Elektrod-elektrod anod kemudiannya melalui proses sepuh lindap pada suhu yang berbeza di bawah keadaan vakum. Sementara itu, bagi kaedah plasma, nilai voltan diubah untuk mengawal keadaan plasma yang mengakibatkan pengubahsuaian pada morfologi permukaan filem nipis. Untuk mencirikan filem berlapis yang dihasilkan, filem-filem nipis ini dicirikan melalui kajian spectroskopi, struktur dan elektrikal. Secara amnya, hasil menunjukkan peningkatan dalam konduktiviti dan kemampubasahan, yang mungkin membuktikan manfaat untuk pelaksanaan di dalam AFCs, dan menggalakkan pertumbuhan alga dengan lebih baik, pelekatan dan fotosintesis yang menyumbang kepada penghasilan mobiliti caj yang lebih tinggi.

Kata kunci: Grafin Oksida Yang Diturunkan, Langmuir-Blodgett Biofotovoltik, Kaedah Plasma, Kaedah Sepuh Lindap.

ACKNOWLEDGEMENTS

First and foremost, praise and thanks to God, the Almighty for giving me strength and ability to accomplish this study. I would not be able to complete this study without His blessings. I have the great pleasure to express my gratitude to my parents and family, Ibrahim Shafie and Umi Kalsom, Abang Yusran and Kak Asma, Abang Zhafran, Abang Khalis and Kak Hajar for their love and prayers to help me to reach this stage in my life.

I would like to express my special thanks to my dedicated supervisor, Assoc. Prof. Dr. Vengadesh Periasamy who consistently and patiently supported me throughout this Master's degree journey and never give up to make sure I complete my study. I would not have completed this writing if it was not because of him. I also would like to thank my co-supervisors Prof. Phang Siew Moi and Prof. Wan Haliza Abd Majid for providing me guidance and support especially in knowledge and financial matters. Not to forget to my super helpful group members Mr. Musoddiq Jaafar, Dr. Victoria, Ms. Siti Zulfikriyah, Nastaran and others for always encouraging and lending hands to help me accomplish this study.

I would also like to express my appreciation for my MyBrain scholarship awarded by the Ministry of Higher Education. The research reported here was supported by the HICoE MOHE: Air-ocean-land Interaction Grant (IOES-2014), IOES UMCoE RU Grant (RU003-2017), FRGS (FP038-2017A), Newton Fund Institutional Link (IF007-2015), and PPP (PG124-2015A) grants.

I would like to express my sincere gratitude to all members and staffs of Institute of Ocean and Earth Science (IOES) and Low Dimensional Material Research Centre (LDMRC), especially Dr. Goh Bong Tong, Ms. Azianty, Ms. Fatin, Ms. Najwa, Mr.

Ariff, Mrs. Norlela and Ms. Linda for their assistance and for providing necessary facilities throughout my journey towards completion of my MSc. I also would like to thank all those who directly or indirectly contributed to the completion of this study.

Last but not least, I am extremely grateful to have continuous physical and emotional support from my best friend, soon to be a Dr. (PhD), Ms. Adilah Roslan. She is a role model and inspiration to me in every single thing she does. Not to forget to mention my husband, Mr. Zulhilmy for always believing in me during the moments I doubt myself.

TABLE OF CONTENTS

LIST OF FIGURES

LIST OF TABLES

LIST OF SYMBOLS AND ABBREVIATIONS

I	:	Current
I_D	:	Intensity Ratio of D Band
I_G	:	Intensity Ratio of G Band
Ω	:	Ohm
π	:	Pi (mathematical constant)
ρ	:	Sheet Resistivity
2-D	:	Two Dimensional
3-D	:	Three Dimensional
V	:	Volume
W	:	Watt
AFCs	:	Algal-Fuel Cells
Al	:	Aluminium
AFM	:	Atomic Force Microscopy
BES	:	Bioelectrochemical System
BPV	:	Biophotovoltaics
C	:	Carbon
CNTs	:	Carbon Nanotube
Chl-a	:	Chlorophyll-a
CVD	:	Chemical Vapor Deposition
Cu	:	Copper
CV	:	Cyclicvoltametric
DC	:	Direct Current
EPD	:	Electrophoretic Deposition Process
ETMs	:	Electron Transfer Mediators

EPS	:	Extra-Cellular Polymeric Substances
FTIR	:	Fourier-Transform Infrared Spectroscopy
FCs	:	Fuel Cells
GCE	:	Glassy Carbon Electrode
GO	:	Graphene Oxide
H_2O_2	:	Hydrogen Peroxide
OH-	:	Hydroxide
ITO	:	Indium Tin Oxide
Fe_2O_3	:	Iron (II) Oxide
Fe_3O_4	:	Iron (II,III) Oxide / Magnetite
LB	:	Langmuir-Blodgett
MFCs	:	Microbial Fuel Cell
Mg^{2+}	:	Magnesium Ion
MIS	:	Metal-Insulator-Semiconductor
Mn	:	Mangenese
NADH	:	Nicotinamide Adenine Dinucleotide
OLED	:	Organic light-emitting diode
O_2	:	Oxygen
PETC	:	Photosynthetic Electron Transport Chain
p-MFCs	:	Photosynthetic Microbial Fuel Cell
PS	:	Photosystem
Pt	:	Platinum
RF	:	Radio Frequency
rGO	:	Reduced Graphene Oxide
RETC	:	Respiratory Electron Transport Chain
Si	:	Silicon

SiC	:	Silicon Carbide
NH^{3+}	:	Trihydrogen Nitride / Ammonia
XRD	:	X-Ray Diffraction

LIST OF APPENDICES

CHAPTER 1: INTRODUCTION

1.1 Background

Graphene, a two-dimensional (2-D) crystal structure found naturally as single layer carbon atoms exhibits unusual electronic properties (Novoselov, 2004) and as such become a material of great interest to scientist. A variety of methods for synthesizing graphene and graphene-derived materials has since been developed for applications in industry (Huang et al., 2018). These include various high-throughput methods of preparing graphene, graphene oxide (GO), and reduced graphene oxide (rGO), deliberately increasing their conductivity, mechanical, thermodynamic, opto-electronic and other properties (Rasuli et al., 2010).

The least conductive or insulating form of graphene derivative, a single layer or few layers of GO is produced from graphite oxide using the exfoliation method (Park et al., 2009). The number of layers greatly differentiates between GO and graphite oxide (Moazzami, 2012), (Li et al, 2008). In addition, due to the presence of oxygen functional groups, GO is easier to disperse in water and other organic solvents (Paredes et al., 2008). Further, as a result of the disruption of its sp^2 bonding networks, GO is usually designated as an electrical insulator. Therefore, in order to achieve electrical conductivity, the reduction of the GO has to be carried-out. There are several methods of reducing GO, for example by exposing GO to hydrogen plasma for few seconds and GO treatment with hydrazine hydrate.

The most preferable method however, is the electrochemical reduction that produces very high quality rGO almost identical to graphene in terms of structure (Loryuenyong et al., 2013). Production of rGO using these techniques created sufficient quantities to

meet increasing demands, which is widely used due to its advantages. For instance, it is economical, involves a facile solution process, enables mass production and allows easy attachment of functional groups (Ng et al., 2014c). Continuous layer of rGO can be deposited using several techniques such as electrophoretic deposition and solution-based methods. However, in recent times Langmuir-Blodgett (LB) technique has been utilized successfully to deposit rGO layers on solid substrates (Jaafar et al., 2015).

LB technique is a method of forming a monolayer or multilayer thin film by transferring a floating substance on an air-water interface onto a solid substrate. The advantage of using this technique is that the number of layers of the film deposited can be controlled with accurate thickness due to the homogenous adsorption of monolayer during the immersion step. In addition, the monolayer substance should be amphiphilic by nature or prepared to be so to allow the substance to be able to float on the water surface. Benjamin Franklin was the first to observe the monolayer phenomenon by virtue of a little drop of oil spreading and covering a large pond. His findings were later reported to the British Royal Society in 1774 (Rayleigh, 1889).

Agnes Pockles later developed a basic surface balance called slide trough to determine the influence of contamination on the surface pressure, and published her first paper with Lord Rayleigh in Nature in 1891 (Rayleigh, 1891). Later in 1917, Irving Langmuir carried-out a systematic study on floating air-water interface monolayer using an improved version of Pockel's slide trough and made additional discoveries pertaining to the properties of surface molecules (Langmuir, 1917), earning him a Nobel Prize in Chemistry in 1932. Katherine Blodgett, a Physicist and Chemist made scientific advance when she demonstrated stacking of several monolayers or Langmuir film on top of each other on a solid substrate to form multilayers (Blodgett, 1935; Malik et al.,

2013). Both Langmuir and Blodgett were later credited for the discovery of the LB trough, which was fundamentally influenced by Pockel's device.

In recent times, one of the most popular technologies involving development of renewable and carbon negative energy is biophotovoltaics (BPV) based fuel cells. In-line with this, various platforms were designed to extract energy from biomaterials such as from algae (Bombelli et al., 2011; Ng et al., 2018). Algae are amongst the best organisms that have potential for alternative energy development. They are one of the most efficient photosynthetic organisms with rapid growth rates, assorted products and tolerance to extreme environment. Biomass productivity of microalgae is estimated to be 50 times higher than switchgrass, being the fastest growing terrestrial plant (Ng et al., 2014c). During photosynthesis process, the radiant energy absorbed by chlorophyll can undergo one of three possibilities; (i) used for photosynthesis (ii) dissipated as heat or (iii) re-emitted as chlorophyll fluorescence (Gray, 2011).

In photosynthesis mechanism, the charge separation takes place during electron transport chain and the energy directly used for biomass production while excess energy released as fluorescence. The graphene derivative rGO has been found to offer unique and biocompatible electrode solutions for anchoring algae and facilitate improved growth while increasing photosynthetic power output when integrated within a BPV platform (Ng et al., 2014c). In our present work, we demonstrate potential in generating renewable energy from local algae strains grown on rGO anodes within a BPV platform, jointly developed with Centre of Research for Electrochemical Science and Technology (CREST), Department of Chemical Engineering and Electrochemistry, University of Cambridge. This type of electrical generation will also reduce carbon footprint and

prove highly advantageous for future energy production while positively contributing towards climate crisis issues.

In this proposal, LB method will be used to fabricate rGO films on glass substrates for growing local strains of *Chlorella sp*. (UMACC 313) in the form of biofilms (electrodes). These optimized electrodes will then be used as anodes in the BPV fuel cell device to acquire and study its electrical outputs.

1.2 Motivation

This section discusses the two factors that motivated the research undertaken in this study. First, there is a need to enhance the biocompatibility of LB-rGO thin films. Secondly, there is a dearth of research on the relevance of LB-rGO thin films as an anode in BPV applications.

The world faces severe challenges caused by overpopulation and massive usage of the main energy resources; fossil fuels (Tschörtner et al., 2019). The depletion of these energy resources led to the development of novel technologies in order to harness and utilize unlimited sources of renewable energy such as solar power (Bombelli et al., 2014; Tschörtner et al., 2019). In these circumstances, bioelectrochemical system (BES) such as microbial fuel cells (MFCs) and BPV may assist in harnessing renewable energy by utilizing living organism to generate electricity (Rabaey et al., 2005; Yang et al., 2011).

BPV is widely used as fuel cells (FCs) by generating electricity, utilizing the light energy to break down a specific photosynthetic component to form molecular oxygen, electrons and protons from water. In the process of electron travel to an anode, the

electrons move through the direct contact of cell by redox proteins or endogenous compound such as exogenous electron transfer mediators (ETMs) (Ng et al., 2017). In developing BPV platforms, most of the studies employed indium tin oxide (ITO) as the anode material for the purpose of charge transfer due to its intrinsic electrical and optical characteristics. For example, a comparative study between ITO and rGO films developed by using LB method has been conducted (Ng et al., 2014c).

They used biological materials (eg. *Synechocystis* cells and thylakoid membrane) in the study and found that the active compounds cannot be sustained for long term operation of a BPV device. In a more recent study, this drawback has been overcome by developing a biofilm on the electrode (cultivated on the electrode surface) of BPV device. The biofilm has a direct contact with the electrode, hence assisting BPV device in reducing internal potential losses. Thus, the BPV device presents a higher power output compared to the previous works (Ng et al., 2014c).

In addition, other materials such as rGO-based transparent conductors (Van Lee et al., 2017) could potentially be utilized as electrode material to improve the efficiency of BPV performance by means of improved biocompatible adhesion with for example algae. Further, large number of pores and roughness of the three-dimensional (3D) layers of LB-rGO thin film may lead towards enhancing the mass transport of materials (Jaafar et al., 2015). Another significant criterion in replacing ITO as the anode material is the higher value of work function where the value for graphene is 4.5 eV meanwhile for ITO, the value is 4.0 – 4.5 eV (Sygellou et al., 2015).

However, the current state of research of BPV platforms yields considerably lower power output compared to conventional fuels cells. As reported earlier (Jaafar et al.,

2015), the performance of the BPV device can be improved by increasing the significant properties of the anode especially in terms of biocompatibilty. As such, in this study, a potential candidate for the anode material in BPV device, LB-deposited rGO thin film is subjected to several treatments in order to enhance its biocompatibility and therefore its device performance.

1.3 Research Objectives

(a) To obtain and optimize rGO thin films using LB technique to improve biocompatibility towards the growth of algae.
(b) To study the structural characteristics of LB-rGO thin films using Fourier Transform Infra-red (FTIR) spectroscopy.
(c) To investigate the optical transparency for the fabricated LB-rGO films.
(d) To investigate the morphology of the LB-rGO thin films using AFM method.
(e) To conduct electrical characterization by generating power and polarization curves and conductivity and resistance measurements on optimized LB-rGO thin films.

1.4 Thesis Outline

The thesis is divided into five chapters. Chapter 1 (Introduction) provides a brief explanation of the background of this research. The objectives and thesis overview were also stated and discussed in this chapter.

Chapter 2 (Literature Review) presents the approach that has been taken in previous works and the important information relating to the current research. An in-depth literature review was carried-out and discussed to understand existing state of research, problem statements and its motivation.

In Chapter 3 (Methodology), the preparation of samples and methods was presented. This includes the characterization techniques used in this project to determine the properties of the samples. The characterization carried-out were Atomic Force Microscopy (AFM) imaging, FTIR spectroscopy, and electrical and water contact angle measurements.

This is followed by Chapter 4 (Results and Discussion) which discusses in detail the results for each characterization studies carried-out. Finally, Chapter 5 (Conclusions and Future Recommendation) briefly summarizes the project outcomes and presents an outlook for future works in LB-rGO films for application in algal-BPV devices.

CHAPTER 2: LITERATURE REVIEW

2.1 Graphene and Graphene-based Derivatives

2.1.1 History and Introduction

In recent years, graphene has drawn widespread attention for various applications such as fabrication of novel composites, transparent electrodes and ultrasensitive sensors (Zhang et al., 2012; Zhang et al., 2010). This is due to the unique mechanical and electrical properties of graphene such as high carrier mobility and ambipolar electric field effects. Graphene is a 2-D structure and has one-atom-thick planar layer in a hexagonal lattice arrangement of sp^2 hybridized bond and it is considered as a large aromatic molecule (Loryuenyong et al., 2013). This 2-D flat sheet can be shaped into zero-dimensional (0-D) by wrapping it up, folded into one-dimensional (1-D) carbon nanotubes and likewise 3-D graphite (Pham et al., 2011). There are many methods in preparing graphene with the required characteristics (Kavitha et al., 2013).

For example, the method of synthesizing graphene includes exfoliation and cleavage, thermal chemical vapor deposition techniques, plasma enhanced chemical vapor deposition techniques, chemical methods, thermal decomposition of silicon carbide (SiC), thermal decomposition on other substrates and un-zipping of carbon nanotubes (CNTs), and other methods (Choi et al, 2010). Most of the techniques involve the reduction of graphite and GO. GO is considered as insulator due to the existence of its functional group (Li et al., 2015). In order to increase the conductivity and allow it to be electrically active, the functional group of GO must be reduced (Mattevi et al., 2009). Up to this time, the chemical reduction method is the most favorable technique to produce graphene sheets. However, due to large mass

production, this promising method cannot utterly remove the significant number of defects and functional groups (Mattevi et al., 2009).

Three necessary steps involved in this process were oxidation of graphite, graphite oxide exfoliation and reduction of GO sheets. First step, oxidizing bulk graphite by chemical oxidation is intended to develop the hydrophilic graphite oxide. Exfoliation of graphite oxide produces monolayers or few-layered stacks of GO by various thermal and mechanical methods e.g. sonication in water. Lastly, GO is reduced into graphene-like material (Loryuenyong et al., 2013).

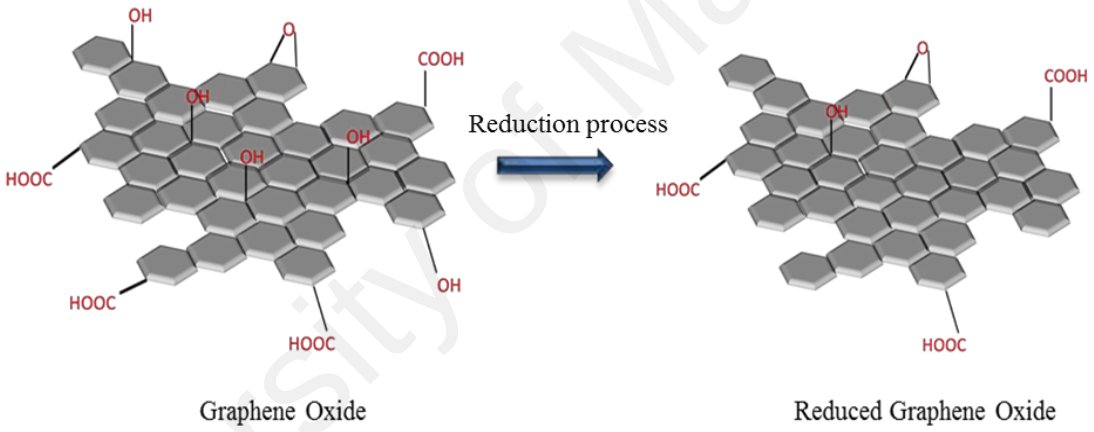

Figure 2.1: Illustration showing the chemical structure of GO after reduction process.

Figure 2.1 shows the chemical structure of GO transformed into rGO after the reduction process. However, during the reduction process, certain parts of the sp^3 structure in the GO were transformed back into sp^2 structure (Sheka et al., 2013). This process could modify the structure, electrical resultant and chemical properties of rGO by varying its strength, duration and method. But still, rGO could not attain a complete sp^2 structure similar to pristine graphene despite the long duration process of chemical reduction. The presence of Stone-Wales defects and holes, which are the loss of carbon and remnant oxygen, caused a limited conversion of this material (Pumera, 2010).

A low electrical conductivity and mildly-reduced sheet presented a high on-off ratio with its transport controlled by voltage-dependent carrier penetrating or leaping between sp^2 clusters (Liu et al., 2012). With an extended reduction of GO, the sp^2 domains did not yield any enlargement in size after oxygen was removed during the chemical reduction process. Otherwise, there was some removal of oxygen moieties while several π-bonds in the carbon were restored. This has resulted in percolation pathways between existing 2-3 nm sp^2 domains in the GO. A high electrical conductivity, which is a heavily reduced sheet, would show a low on-off ratio with ambipolar properties. In spite of the massive reduction process, the electrical conductance in rGO was still subjected to limitations due to the restricted number of potential conduction pathways and the fixed size of sp^2 domain (Liu et al., 2012).

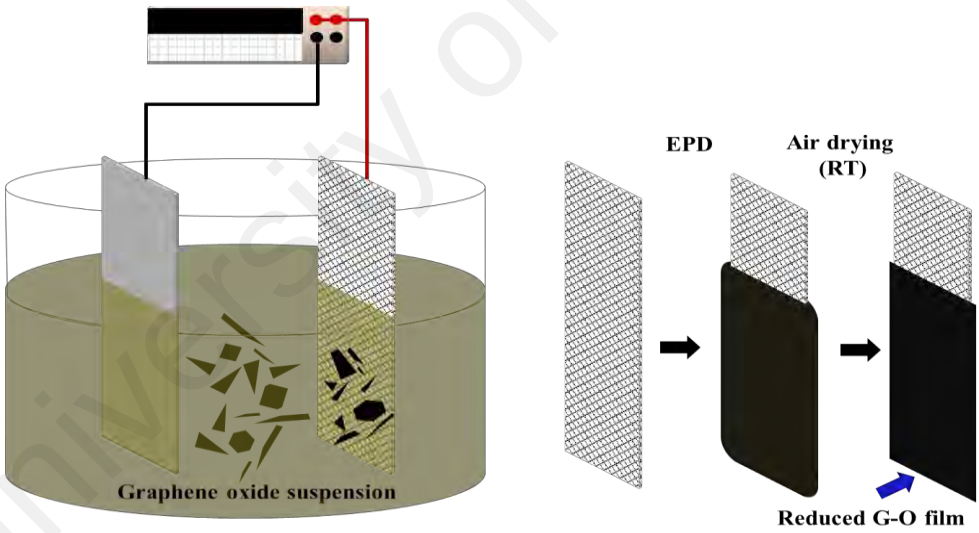

Figure 2.2: The EPD set-up. Adapted from "Thin Film Fabrication and Simultaneous Anodic Reduction of Deposited Graphene Oxide Platelets by Electrophoretic Deposition" by An et al., 2010, *The Journal of Physical Chemistry Letters*, *1*(8), p.1259-1263. Copyright 2010 American Chemical Society.

There are many types of rGO thin film deposition. For example, (An et al., 2010) stated that rGO platelets were produced from GO after undergoing an electrophoretic deposition (EPD) process. Figure 2.2 shows the EPD set-up and when direct-current

(DC) voltage was applied, the GO platelets were drifted to the positive electrode. The EPD-GO thin film was deposited on various types of substrates for example stainless steel, copper (Cu), aluminum (Al) and p-type silicon (Si). As the similar experiments were conducted, the deposition time of EPD-GO deposited onto p-type-doped Si substrate was five (5) times higher compared to stainless steel substrate. However, the different deposition time resulted in the same layer of thickness for both substrates. In the case of the stainless-steel substrates used in this experiment, it was reported that the formation of metal hydroxides experience suppression at the electrode (Thomas et al., 2005).

In another work (Eda et al., 2008), described the deposition of rGO thin film by using vacuum filtration method. In this technique, 25 nm pores sized mixed cellulose ester membrane act as a filter agent to allow the GO sheets suspension to undergo the filtration process. The deposited GO film on the ester membrane is needed to be shifted onto another substrate by placing the GO film directly on its surface. The films are well adhered to the substrate and the ester membrane is then removed by using acetone solution.

2.1.2 Applications in Modern Electronics

The most challenging part in this work is to determine the process of fabricating rGO similar to pristine graphene. However, the fascinating properties of rGO are highly considerable for electronic devices. It has a moderate conductivity having a similar behaviour to semiconductor material besides being able to be made significantly thin (Zhu et al., 2010; Chen et al., 2012). There are many applications involving rGO in electronic devices. For example, rGO have been used in electronic devices (Huang, 2012; Lightcap, 2013), in energy storage (Lightcap, 2013), and polymer composite

materials (Huang, 2012) as well as in biomedical applications (Sun et al., 2008; Chung et al., 2013). Liu and co-workers (Li et al., 2012) reported that rGO sheets are excellent candidates for electrochemical detection application. By virtue of the novel rGO electronic structure, especially the high density of the electronic states over a large energy range, it has been indicated that the electron transfer rate of $Fe^{3+/2+}$ on rGO is higher than on a glassy carbon electrode (GCE) (Tang et al., 2009; Zuo et al., 2010). Likewise, in enzyme-based sensors, rGO has intrinsic catalytic activity towards tiny enzymatic products such as Hydrogen Peroxide (H_2O_2) and Nicotinamide Adenine Dinucleotide (NADH) thus, make this superior material convenient for the device (Zhong et al., 2010). Besides offering a huge area of effective reaction, rGO-based electrodes also provide a high capacity for enzyme loading.

In lithium ion batteries, rGO nanocomposites have been used for large capacity energy storage (Wang et al., 2008; Zhang et al., 2010). These works studied insulating metal oxide nanoparticles which was adsorbed onto rGO to enhance the efficiency of the materials in the working batteries. For example, using iron (II,III) Oxide (Fe_3O_4) on rGO versus pure Fe_3O_4 or iron (II) Oxide (Fe_2O_3) increased energy storage capacity and cycle stability (Zhou et al., 2010). In supercapacitors, this high surface area rGO works as an energy storage material (Zhu et al., 2011; Zhu et al., 2010). The dominant use of rGO in electrochemical sensors is due to its abundant defects and chemical groups that assist the progress of charge transfer and hence establish high electrochemical activity (Kumar et al., 2013). Sensor performance can be enhanced due to the existence of chemical moieties on the rGO surface that offer the convenience and flexibility for several functionalizations. In addition, rGO is highly tunable in chemical and electrical properties and it can transport charges efficiently as compared to non-conductive GO.

2.2 Langmuir-Blodgett

2.2.1 History of Langmuir Blodgett

As introduced in Chapter 1, LB technique allows successful transfer of a floating amphiphilic monolayer of molecules on top of a liquid surface or subphase onto a solid substrate. It is one of the most promising techniques for large-scale thin film deposition without the need for any hazardous materials. In 1977, Benjamin Franklin dropped a teaspoon of oil onto a pond's surface and observed a calming effect without realizing that the formation of a monolayer of oil on the surface was responsible for the effect (Rayleigh, 1889). Lord Rayleigh quantified it over a century later and calculated the thickness at 1.6 nm (Roberts, 2017). Agnes Pockles later was the first person to measure the effect of impurities on the surface tension of the liquids. Irving Langmuir then continued this study with the help of Katherine Blodgett who discovered that the monolayer of the molecule could be transferred onto a solid substrate (Malik et al., 2013).

The basic of LB thin film deposition process such as surface tension, surface pressure, insoluble monolayer and isotherm graph must be understood prior to commencing the deposition process. For LB deposition method, materials that comprise of strong hydrophilic and hydrophobic groups, termed amphiphilic molecules will naturally form a monomolecular film at the water surface (Roberts, 2017). Molecules can be classified into either hydrophilic, hydrophobic or amphiphilic by nature. In amphiphilic molecules such as the oil used in Benjamin Franklin's experiment, the hydrocarbon chains are the hydrophobic or "water-hating" part while the polar groups (OH^-, NH^{3+} etc.) are the hydrophilic or "water-loving" part of the molecule (Shaw, 2013). The properties of amphiphilic material can be ascertained by the water surface pressure of the molecules by means of an isotherm. By decreasing the surface area

through compression of LB barriers at constant rate, the isotherm can be generated. The isotherm for a typical fatty acid is shown in Figure 2.3. From this figure, three different phases of molecular stages can be visualized; i.e. gas (G), liquid (L), and solid phases.

The distance between molecules during gas phases are large and attractive forces between them are weak. During liquid phases, the distance between molecules becomes closer to one another and some of the molecules start to collide upon increasing the surface pressure by means of the compressing barriers. On the other hand, these phenomena also resulted in higher attractive force between the molecules. By further increasing the surface pressure, the molecules will reach the solid-state stage and begins to form a well-arranged monolayer on the water surface. Further compression and higher surface pressure will cause the molecules to collapse at the break point by overlapping other neighbouring molecules. At this stage, the surface pressure or collapse pressure was observed to rapidly decrease (Das et al., 2017).

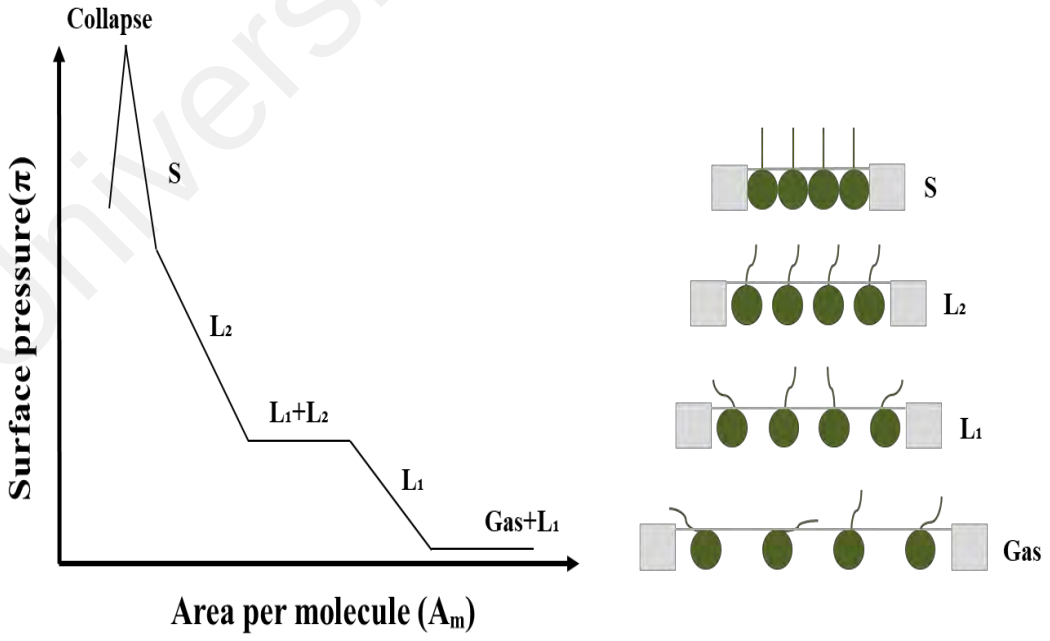

Figure 2.3: A typical isotherm for fatty acid. Adapted from "Molecular interactions at interfaces" by R. Gupta and V. Manjuladevi, 2012 (https://www.intechopen.com). Copyright 2012 InTech.

In LB technique, there are two approaches for thin film deposition i.e. horizontal and vertical depositions (Niinivaara et al., 2016) as shown in Figure 2.4. In the horizontal position, the amphiphiles on the water surface are transferred to the substrate by placing the substrate horizontally on the water surface. Meanwhile, in the vertical deposition, the substrate is dipped and slowly moved up in the vertical direction out of the water surface usually using a controlled computerized system.

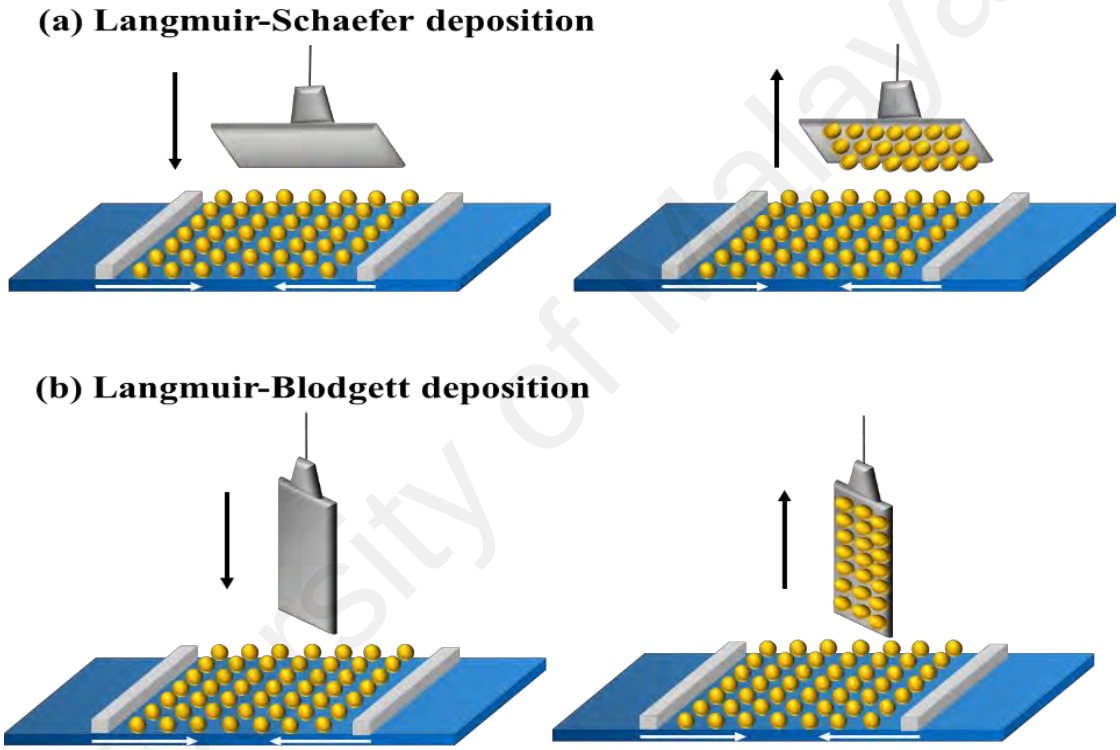

Figure 2.4: The horizontal (a) and vertical (b) deposition using Langmuir Schaffer (LS) and LB methods, respectively. Adapted from "Parameters affecting monolayer organisation of substituted polysaccharides on solid substrates upon Langmuir–Schaefer deposition" by Niinivaara et al., 2016, *Reactive and Functional Polymers*, *99*, p. 100-106. Copyright 2016 Elsevier.

As reported by Agnes et al., the significance of this highly promising thin film preparation is that it increases the accuracy of the monolayer's thickness. Besides, the possibility of a homogenous deposition over the large area of thin films is high and it is transferable to many kinds of solid substrates (Blodgett, 1935; Kalinowski, 1999;

Niinivaara et al., 2016). In addition, the varying layers of composition can be achieved by optimizing this technique.

Due to the uniqueness of the amphiphile molecules' self-assembled characteristics on water surfaces, this technique offers a promising result in preparing biomimetic layers for bio-active immobilization of molecules (Girard-Egrot et al., 2007). A monolayer of gold nanoparticle fabricated using this method has been integrated into a metal-insulator-semiconductor (MIS) structure (Paul et al., 2003). The pre-requisite for molecular electronic devices is organized molecular assemblies, which is almost exclusively offered by the LB method. This is considered as the prior example of 'supramolecular assembly', where the molecular level of control can be applied in organic thin films structure (Kuhn et al., 1971).

2.2.2 Graphene-based Langmuir-Blodgett Thin Film and its Applications

As previously reported, rGO layer was deposited on ITO surface using LB method to assure the control of thickness (Yang et al., 2014). In addition, LB technique could also ensure the defined structure of the rGO layer being transferred onto a substrate, working well as an effective hole injection layer (Eda et al., 2008; Tan et al., 2013). Besides, rGO has been used as electrode layer for organic photovoltaic devices and organic light-emitting diode (OLED) due to its specific electrical properties and high transparency (Yin et al., 2010; Gao et al., 2011).

In another work, it was reported that graphene-based monolayers have been prepared by utilizing pH dependent LB assembly of GO sheets (Cote et al., 2010). The deposited monolayers were dominated by two basic morphological features; wrinkles and overlapping graphene sheets. These morphological features have been found to

impart significant effects on the electrical and optical properties of the thin film. Therefore, the LB technique is a favorable method to allow significant control in terms of layer thickness and wrinkles for fabricating conductive modified graphene. These features prompted their characteristics to be extensively studied in order to optimize the properties of optoelectronic devices (Kim et al., 2013).

2.3 Algae

2.3.1 Introduction

Algae are categorized as plants with lack of roots, stems and leave and generally contain chlorophyll-a as its primary photosynthetic pigment (Blankenship, 1998; Lee, 2008). Algae can easily be found in almost every place on Earth including in the harshest regions of extreme temperatures. Algae are also commonly found in fresh, marine or even in brackish water (Demirbas et al., 2011) and are in the food chain of most habitats forming the basic food source (Lee, 2008). Algae cells are categorized into two types; prokaryotic and eukaryotic. Prokaryotic cells are unicellular organisms without a true nucleus and chloroplast enveloped by a membrane. Meanwhile, eukaryotic cells are more complex with membrane-bounded organelles and multiple chromosomes which have the capability to generate its energy through mitochondria and other systemic functions (Lee, 2008).

Based on several criteria including pigment composition, algae can be divided into several types such as chromista, red algae and green algae. Chromista type of algae consists of chlorophyll a (Chl-a) and c which can be found in brown algae, kelp and diatoms. These types of algae have multicellular structure and thrive in the open seas as well as rocky coasts (Lee, 2008). Meanwhile, marine algae (seaweed) are an example of red algae type which contains chlorophyll a and phycoerythrin, a red pigment. They act

as the food resources for marine species and can be found in plenty in tropical areas and warm waters. This type of algae consists of phycobilins (red) mask chlorophyll a and accessory pigments (Lee, 2008). The next type is the largest and most diverse algae group; green algae. Chlorophylls a and b are present in this type of algae. Some of the green algae has a similarity feature to terrestrial plants, where both have a cell wall made of cellulose. The green algae type has single cells (eg. *Micrasterias*) structures, filamentous algae, colonies (eg. *Volvox*), and leaf-like shape (*thalli*) (eg. Ulva). These green algae species can be abundantly found in fresh waters and on the land for instance epiphytic rocks, trees and soil (Lee, 2008).

2.3.2 Chlorophyll-a

Chlorophyll consists of a long hydrophobic chain made up of porphyrin ring with magnesium ion (Mg^{2+}) at the center which gives green pigments to the organelle. The green pigments are the major component for the light absorption in photosynthesis process. Generally, chlorophylls can be classified to chlorophyll a, b, c and d which can be differentiated by the side-chain substitutions. Chl-a are the most commonly found especially in microalgae (Morançais et al., 2018). Also, this photosynthetic pigment Chl-a are usually identified in all known oxygen-evolving organisms. Most of the oxygenic photosynthetic organisms' oxygen production mechanism is commonly similar involving Chl-a separating charges in the actual conversion of water into molecular oxygen (Blankenship, 1998).

2.3.3 Importance of Algae

Majority of algae species are categorized as phototrophs and light is their basic need for growth. As reported earlier (Patil et al., 2005), these phototropic microalgae are generally grown in open ponds and photobioreactors. The open pond cultures are more

favorable due to the economical aspect however it may raise certain issues regarding to the land cost, water availability, and climate conditions. Microalgae have various advantages compared to other crops. For instance, they have high growth rates and photosynthesis efficiencies, high in oxygen (O_2) production and can be grown in non-arable area (Gouveia, 2008). Recent researches had demonstrated great potential in biodiesel production where the oil extraction processes are mostly concentrated on the microalgae as huge bioenergy sources (Brennan et al., 2010; Chisti, 2007).

The quantities of algal biomass must be plentiful in order to produce large quantities of microalgal biodiesel. (Demirbas et al., 2011) reported that the biomass from dried microalgae and commercialized in the form of powder as a supplement for human consumption are applicable to act as co-firing in order to generate electricity, produce bio-oil through pyrolysis as well as producing biomethane via fermentation. On the other hand, biomethane can also be obtained from marine biomass. Besides, they are also known as one of the effective solar energy converters. Various metabolites can be attained from these microalgae (Demirbas et al., 2011; Campbell, 2008).

In recent times, many companies had invested in microalgae biofuels as it is highly potential to produce fuels for the transportation sector such as biogas and aviation fuel (Milledge, 2014). However, the rising financial value is the main circumstances for algal biofuels implementation. In order to ensure algal biofuels to be more cost effective, the extraction of any varied precious products from algae or integrating their production into waste-water treatment are highly recommended options (Gouveia, 2008; Milledge, 2014). Both micro- and macroalgae has also been reported to be rich in polysaccharides (PS) and majority of them being sulphated compounds (sPS) (Maria, 2015). These fascinating compounds have a huge potential in health benefits

pertaining to the application of therapeutics, pharmaceuticals and regenerative medicine. Besides, the other bioactivities that can be performed by PS include the immunomodulatory ability, antitumor and cancer preventive activity (as anti-proliferative agents, tumor suppressors or natural cell-killers). In fact, they are also rich in antioxidants as well as antibiotics and anti-inflammatory agents.

2.4 Biophotovoltaics

2.4.1 Introduction

Biological BPV devices or photo-microbial fuel cells regarded as "living" solar cells are the type of devices that generate electricity from the biological process of living organism. In algal-BPV systems, electrons triggered and generated from the photolysis of water during the photosynthesis process will be transferred to an anode. High potential reaction relatively takes place at the cathode and potential difference drives the current through an external circuit.

On the other hand, MFCs are also applicable in various applications such as wastewater treatment, sensors, remote power source, value-added compounds production via electrosynthetic and electrochemical processes. This potential application of MFCs also includes utilization as a research platform to study the fundamental microbial respiration (Angioni et al., 2018; Lee et al., 2015; Pandit et al., 2015). Figure 2.5 shows the schematic diagram for a MFC, which generally use bacteria as the material in the anodic chamber of the device. The anodic chamber's surface area is high to efficiently allow the bacteria to form a biofilm and usually the condition is anaerobic for the bacteria to function (Rahimnejad et al., 2015; Najafpour et al., 2011).

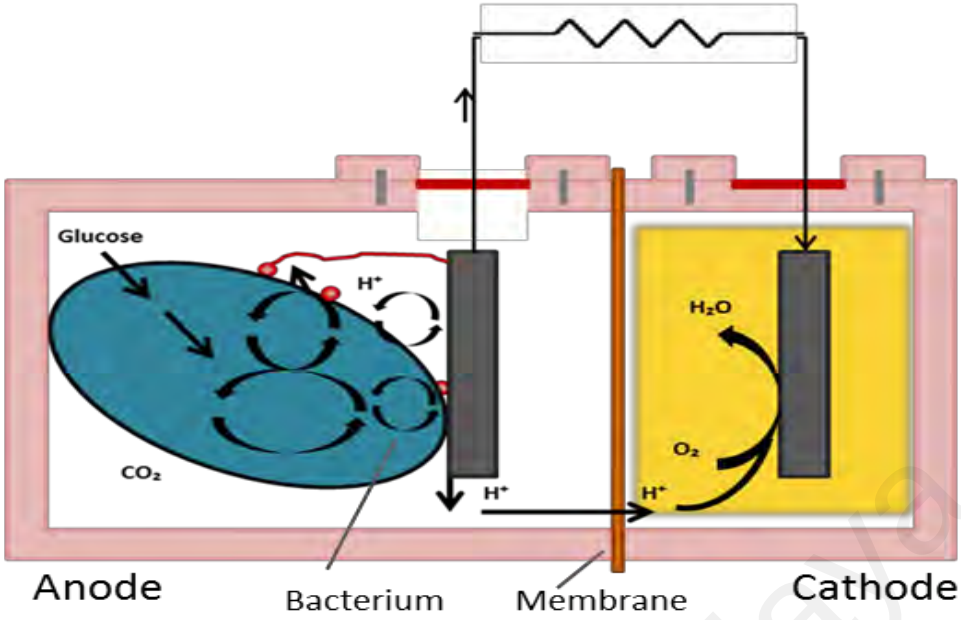

Figure 2.5: The schematic diagram for Microbial Fuel Cells (MFCs). Adapted from "Microbial fuel cells: Methodology and technology" by Logan et al., 2006, *Environmental Science & Technology*, *40*(17), p. 5181-5192. Copyright 2006 American Chemical Society.

The process of organic molecules being broken down by the bacteria in the electrolyte results in the production of electrons which are then transferred to the anode. The efficiency of electron harvest is high, and reports of a 90% efficiency using organic compounds have been reported (Mathuriya, 2014). However, there is a drawback in this application where the production of carbon dioxide is high due to the bacterial respiration (Logan et al., 2006). While in a photosynthetic microbial fuel cell (pMFCs), microorganisms can also donate electrons to the anode through the catabolism and photosynthesis (Chiao et al., 2006; Ryu et al., 2010). One of pMFCs primary advantages draw interest in research field as a self-sustainable way of creating energy.

Additionally, due to photosynthetic carbon segregation, the probability of carbon neutral energy production is also highly possible. Previous works that many groups of photosynthetic materials such as sub-cellular, eukaryotic (algae), prokaryotic (cyanobacteria), and mixed systems have been used in the anodic chamber (Gude et al.,

2013). The part of sub-cellular organelles such as photosystems I (PS I) and II (PS II) (Maly et al., 2005; Badura et al., 2006), thylakoid membranes (Lam et al., 2006), isolated chlorophyll and bacterial reaction centers was included (Janzen et al., 1980). However, pMFCs incorporating organelles deal with a short lifetime since the organelles do not have the ability to self-repair (Malik et al., 2009).

The MFC device demonstrated an effective method in generating electrical power by the organic compounds and chemical fuels. This development of MFC has inspired BPV device to produce electrical power through photosynthetic organisms by studying their biological activities. Even though the study has potential, there are limitations for the full utilization and exploitation of these devices, in particular, the needs of anaerobic conditions in the anode, an applied bias potential and oxygen enrichment at the cathode (Bombelli et al., 2011).

In recent studies, the development of biofilms in BPV device has shown improvement in the power output results. The biofilms were cultivated on the surface of electrode in BPV devices and this condition cause the direct contact between the cell and the electrode and hence, resulting in low rate of internal potential losses (Ng et al., 2014b).

2.4.2 Types of Biophotovoltaic Platforms

Two types of substrates; glass and ITO were chosen to compare the adhesion quality of algae biofilm formation on the surface. They have different characteristics where the glass substrate has high surface energy and considered a hydrophilic material while ITO is hydrophobic and has low surface energy (Ozkan et al., 2013). ITO was a favourite

hole injection cathode as it exhibits good conductivity and transparency (Hwang et al., 2006), prompting the motivation for application in MFCs to yield good quality biofilms.

The types of algae found suitable in BPV application are *Chlorella* sp. (UMACC 313) and *Spirulina platensis* (UMACC 159) (Ng et al., 2014a). These two types are capable in forming biofilms on the ITO anode. The *Chlorella* biofilms coverage on the anode platform is 99.46% and the maximum relative electron transport rate (rETRmax) is 140.796 μmol electrons m^{-2} s^{-1}. Meanwhile, the *Spirulina* records 80.70% and 153.507 μmol electrons m^{-2} s^{-1} for the biofilm coverage and maximum relative electron transport rate (rETRmax), respectively (Ng et al., 2014b). These results indicate the potential of these microalgae to generate electrical energy when integrated within BPV platforms.

2.4.3 Algae Fuel Cells

Solar energy is a great source of sustainable resource among other methods due to the massive amount of energy constantly and fairly distributed by the Sun to the Earth (Zhu et al., 2008). In addition, this abundant and cost-effective energy source can be completely utilized as long as it is converted to other energy for various applications. Many favorable artificial devices, for instance, silicon-based solar cells have been studied further and industrialized. Nevertheless, there are several drawbacks regarding this invention especially pertaining to the cost-effectiveness of the production as well as the raw material, inadequate operation time and its sustainability (Leong et al., 2009).

Thus far, utilization of photosynthetic material in the production of fuels manufactured from organic material and biofuels are the leading approach for harnessing solar energy (Smith et al., 2011; Gouveia et al., 2009). Photosynthetic

species are a good candidate to exploit in capturing energy from renewable source since it is greatly adapted to convert solar energy to chemical energy along with the large abundance of this species in this world (Cho et al., 2008).

2.5 Significance of Study

The findings of this study will play an important role to improve the performance of the BPV device. Further characterization of LB-rGO thin films are required to examine the potential of this thin film as an improved anode. The enhancement of the related characteristics such as the functional groups, the morphology, the conductivity and the hydrophilicity will be studied and optimized in this work, promoting higher value of power output. Therefore, the optimization of LB-rGO thin films will further facilitate the improvement of the relevance of LB-rGO thin films as an anode hence resulting in higher performance of BPV devices.

CHAPTER 3: EXPERIMENTAL METHODS

3.1 Introduction

In this chapter, the experimental techniques and methods used will be discussed in detail starting with the preparation of rGO solution (Section 3.2) followed by rGO deposition (Section 3.3). Section 3.4 discusses about the treatment for the thin film while the following Sections 3.5 and 3.6 provide detailed explanation of algae cultivation and chlorophyll extraction, respectively. Lastly, the characterization method is discussed in Sections 3.7 until 3.11, which include measurement of sheet resistivity, measurement of contact angle, electrical characterization and FTIR characterization.

3.2 Preparation of rGO solution

The experiment was conducted in a dust-free 1K clean room (ISO Class 6). 2.0 mg of rGO (Graphene Supermarket, USA) was mixed with 1.0 ml of polar solvent (99.9% pure methanol in a 5.0 ml vial). The vial was sealed securely and sonicated up to 10 hours using Thermo-6D Ultrasonic Bath (40 kHz).

3.3 rGO Deposition Using Langmuir-Blodgett Method

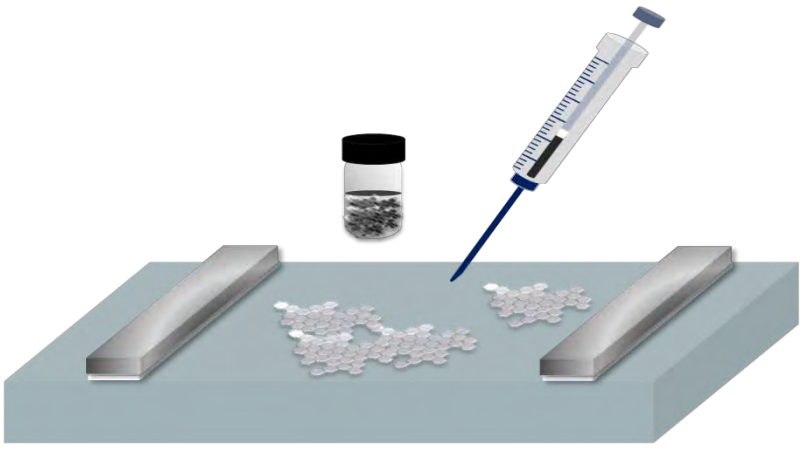

Figure 3.1: Preparation for Langmuir-Blodgett rGO deposition.

Figure 3.1 illustrates the process of applying rGO solution using a microsyringe drop by drop onto the water surface. Subsequently, the isotherm process for rGO is obtained in order to get the appropriate value of surface pressure such that the rGO monolayer can be transferred onto the glass substrate. The polytetrafluoroethylene (Teflon) component of round-type NIMA LB trough (model 2200) from Nima Technology, UK as shown in Figure 3.2 was pre-cleaned using trichloromethane.

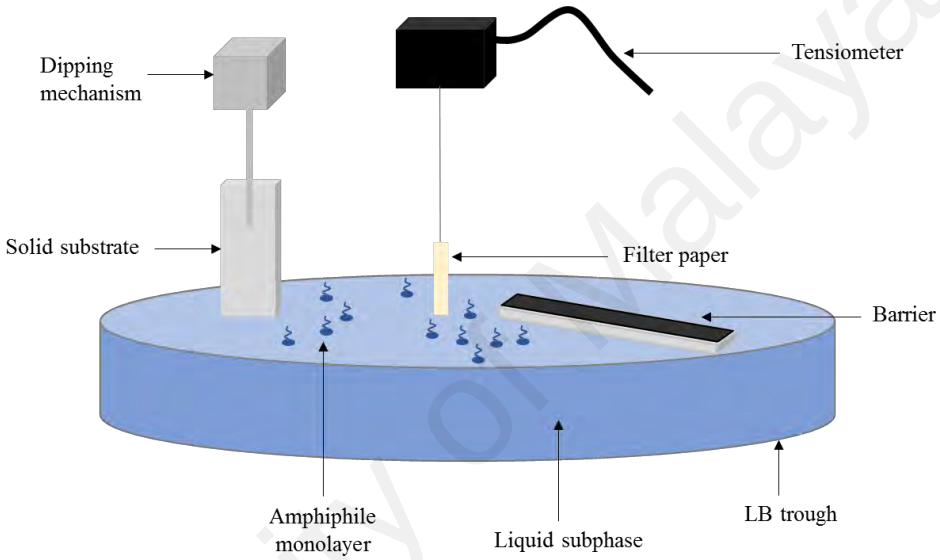

Figure 3.2: The schematic diagram of round LB trough.

Dust particles on the water surface were softly removed using a pipette connected to an aspirator pump (NIMA LB model 2200, UK). 1000 µl of rGO solution was spread drop by drop within one-minute interval to avoid molecular aggregation. To ensure the solvent is fully evaporated, the system was left for about 15 minutes to self-stabilize. The barriers were compressed at about 15.0 cm²/minutes until the reading of surface pressure of rGO shows a target pressure of 1.0 mN/m. During compression of the barriers, surface pressure was monitored by a tensiometer attached to a filter paper of dimensions of 1.0 cm x 2.2 cm (Jaafar et al, 2015). At the target pressure, the rGO layer was deposited vertically onto a glass substrate (3.5 cm x 3.5 cm) with a speed of 20

mm/minute. The film was then dried in the oven at 80°C up to 12 hours in order to increase its adhesiveness towards the substrate. For this work, LB rGO deposition process was repeated 6 times (Ng et al., 2014c).

3.4 Sample Treatment Process

3.4.1 Annealing Treatment

For annealing treatment process, different temperatures; 200 ˚C, 250 ˚C, 300 ˚C, 350 ˚C and 400 ˚C were applied to prepare the rGO films using a tube furnace (Model FA21130-33). The temperature for annealing treatment process was chosen to start at 200 ˚C due to the significant changes in its characteristics between 150 ˚C and 250 ˚C (Lei et al., 2017). The furnace was vacuumed for 2 hours to allow the air to pump out and the sample annealed for a period of 20 hours.

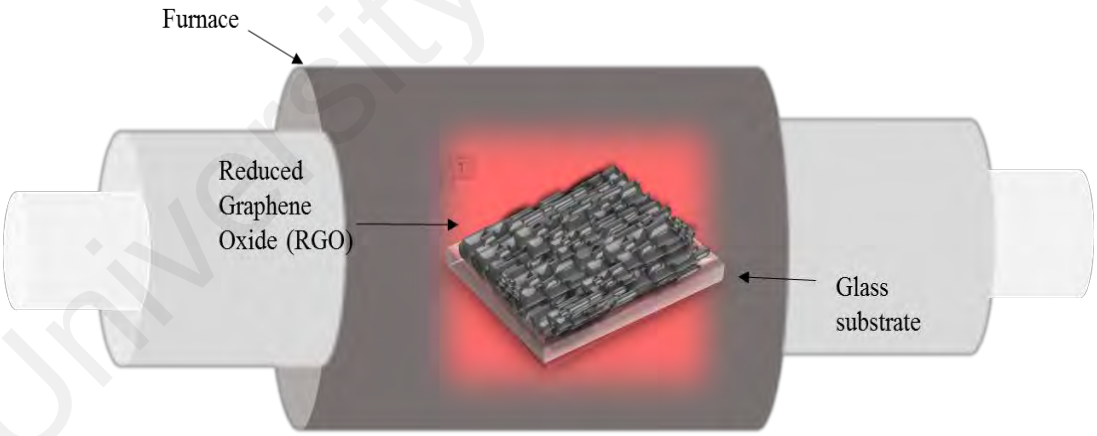

Figure 3.3: The schematic diagram of annealing process in tube furnace.

3.4.2 Plasma Treatment

By using chemical vapor deposition (CVD) system, the LB-rGO thin films were treated with varying plasma power of 20, 60, 100 and 140 Watt (exposed under Argon

ambience for 10 minutes with 90 sccm of flow rate) restricted only by the limitations of the settings of the plasma chamber.

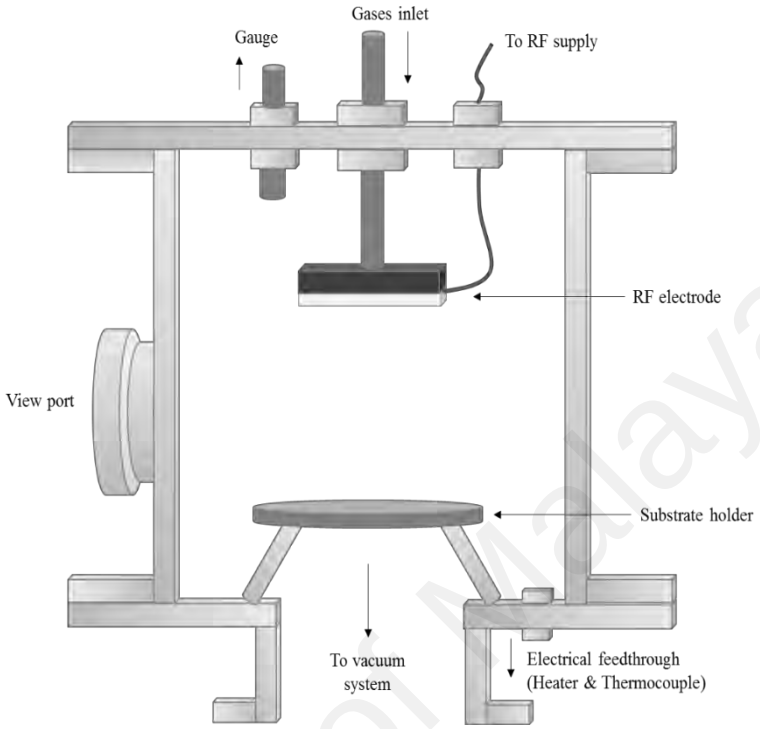

Figure 3.4: The schematic diagram of plasma treatment in CVD system.

3.5 Device Fabrication

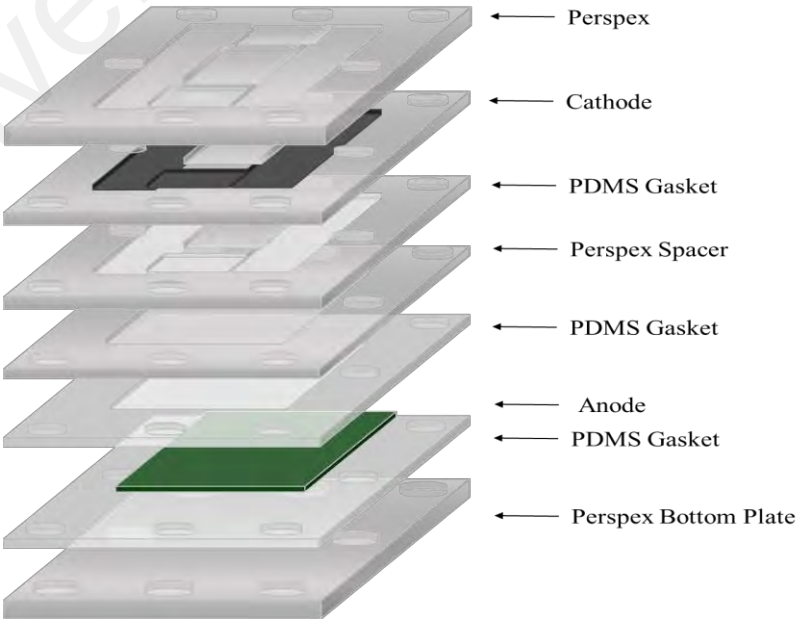

Figure 3.5: Exploded diagram of the BPV device used in this work.

Figure 3.5 shows the exploded diagram of the BPV device fabricated for this work. It consist of a Platinum (Pt)/Carbon (C) cathode and the rGO anode coated with the algae *Chlorella sp*. (UMACC 313) biofilm as prepared in Section 2.2. Proper electrical connection were made using adhesive copper tapes. Power density (Wm^{-2}) for each Argon plasma treated and non-treated algal/rGO anode was measured as 30 µmol.photons.$m^{-2}s^{-1}$ of light irradiation. Further cyclicvoltametric (CV) and chronoamperometry measurements were carried-out using selected plasma treated anode with the highest power density generation.

3.6 Algae Cultivation

Green algae *Chlorella sp*. (UMACC 313) is a potential species for biofilm and was selected from University Malaya Algae Culture Collection (Phang, 1999). This species was grown in Bold Basal Medium (Brown et al., 1964) and 100 ml of an exponential phase culture with Optical density (OD_{620nm} = 0.5) were used and placed in a sterile glass staining jars (100 ml). The prepared LB-rGO thin films was then immersed into the jars containing the algae culture. The jars were then kept in an incubator under 12:12 hours light-dark cycle at 24 °C illuminated by white fluorescent lamp (30 µm.$m^{-2}s^{-1}$) for a total of 15 days. This allows optimum growth of the algae biofilm on the rGO film.

3.7 Extraction of Chlorophyll-a

By using the colorimetric technique demonstrated by Strickland and Parsons (1976), the chlorophyll-a (Chl-a) concentration was calculated. The rGO-algae biofilms were rinsed in 20 mL distilled water and filtered on glass-fibre filters (Whatman GF/C, 0.45 µm). The filtered sample was then mixed with 10 mL of 100% acetone before being mashed in a polypropylene centrifuge tube using a glass rod. Further, the tube was sealed with an aluminum foil and kept in a 4 °C chiller for 24 hours. The sample was

centrifuged on the next day for 10 minutes at 3000 rpm. The extracted absorption was measured at 665 nm (OD_{665}), 645 nm (OD_{645}) and 630 nm (OD_{630}) with three repetitions. To calculate the Chl-a concentration, the following equations 3.7.1, 3.7.2 and 3.7.3 were used;

$$\text{Chl-a (mg mL}^{-3}) = \frac{C_a \, x \, V_a}{V_c} \tag{3.7.1}$$

$$\text{Chl-a (mg L}^{-1}) = \frac{Chl{-}a \; (mg \; m^{-3})}{1000} \tag{3.7.2}$$

where C_a is given by;

$$(11.6)(OD_{665}) \; - \; (1.31)(OD_{645}) \; - \; (0.14)(OD_{630}), \tag{3.7.3}$$

V_a is the volume of acetone (mL) used for extraction and V_c is the volume of culture (mL).

3.8 Measurement of Sheet Resistivity

A four-point probe (Jandel Universal Probe Station, USA) was used to determine sheet resistivity of material. The sample is placed carefully and all the probes were ensured to touch the surface of the sample. During the measurement, current is passed through two outer probes while the voltage is induced through the two inner probes. Hence, the resistance of the material is measured. The sheet resistivity is calculated by using the equation 3.8.1 (Smith, 1958) below;

$$\text{Sheet resistivity, } \rho \left(\frac{\Omega}{sq}\right) = \frac{\pi}{\ln(2)} \text{ x } \frac{V}{I} \tag{3.8.1}$$

where V (volt, V) is the voltage across inner probes and I (A) is the current in the outer probes.

3.9 Measurement of Water Contact Angle

OneAttension is software used to identify the behavior and measure the contact angle of water droplet on the rGO layer after annealing and plasma treatments. The samples were placed on the instrument's platform aligned with the camera. Approximately, 3.5 µL of water were dropped on the sample's surface and the photograph of the contact angle was recorded.

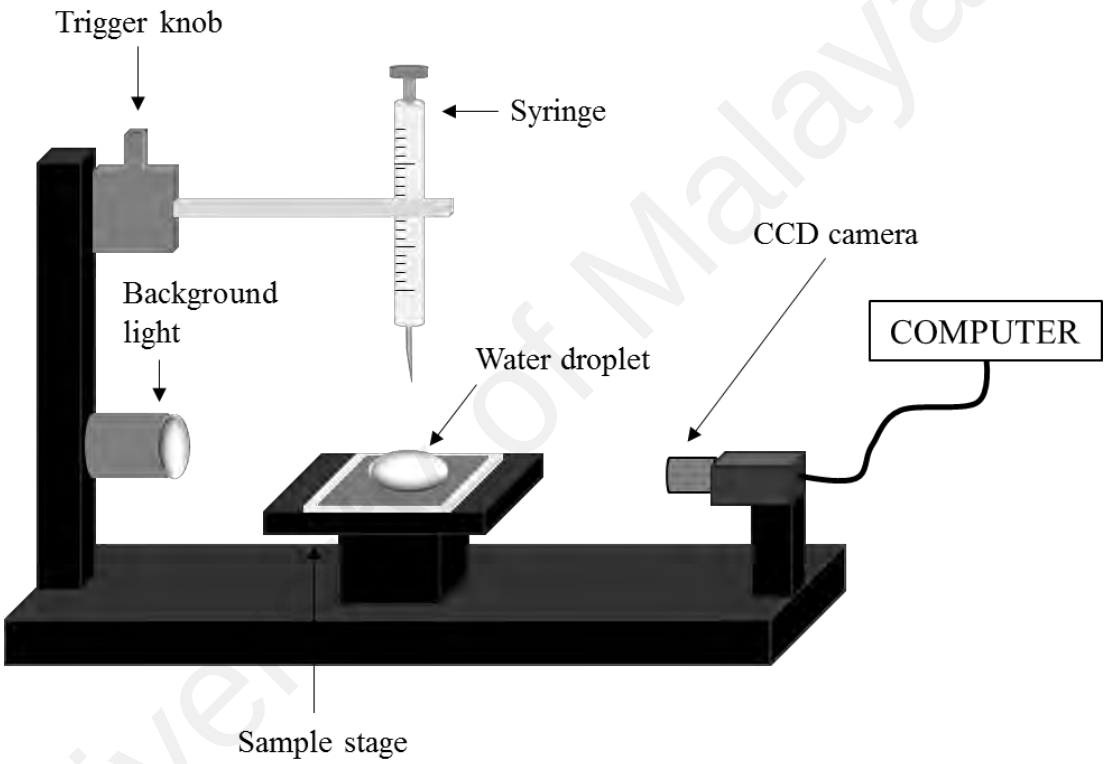

Figure 3.6: The schematic diagram of the instrument to measure wettability.

3.10 Electrical Characterization

For electrical measurement, the devices were placed in the light condition illuminated by a fluorescence light source with irradiation of 30 $\mu m.m^{-2}s^{-1}$. While in dark condition, the devices were covered by a black cloth. A light meter (LI-250A, Licor) was used to make sure the dark condition of the surrounding is zero light intensity. The devices were left for 15 minutes for dark or light condition adaptation

before any readings are taken. Current output was measured by using a multimeter (Agilent U1251B) and different resistance loads (10 MΩ, 5.6 MΩ, 2 MΩ, 560 KΩ, 240 KΩ, 62 KΩ, 22 KΩ, 9.1 KΩ, 3.3 KΩ and 1.1 KΩ) were applied during the measurement for acquiring polarization curves of the BPV devices. All measurements were conducted in triplicates to ensure the reproducibility and improve the statistical significance of the experiment.

3.11 Sample Characterization

Fourier Transform Infrared (FTIR) from Perkin Elmer (FTIR-Spectrum 400 Spectrometer, USA) is a technique used to obtain the infrared spectrum of emission, absorption, photoconductivity or Raman scattering of solid and liquid. FTIR spectrometer simultaneously assembles spectral data in a wavelength range of 4000 cm^{-1} to 400 cm^{-1}. In this experiment, each sample was characterized using FTIR technique to observe the ratio of oxide group post-annealing and after plasma treatment. The FTIR spectra was recorded after three times of readings. The schematic diagram of FTIR Spectrometer is shown in Figure 3.7.

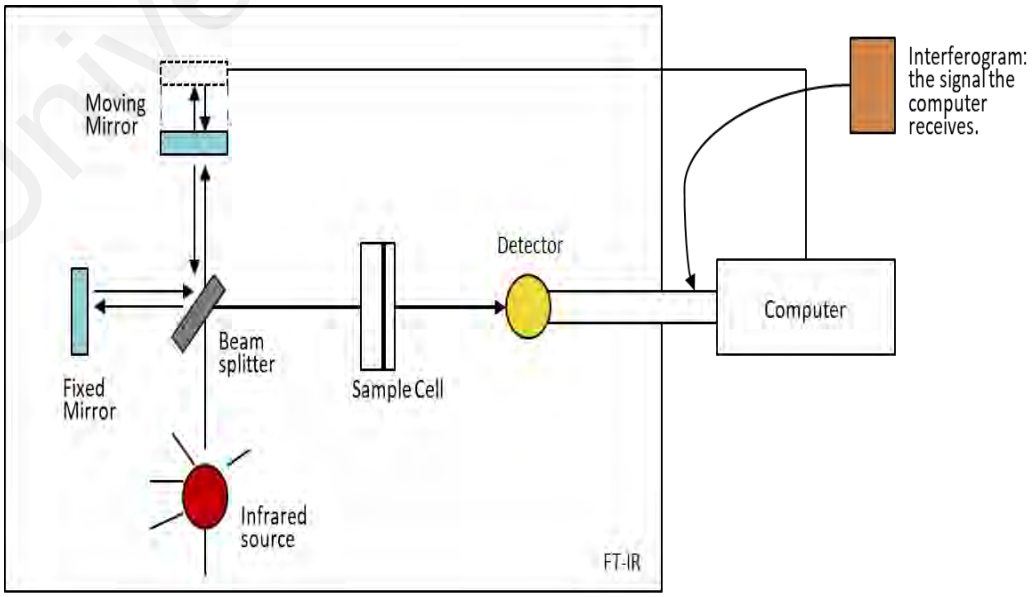

Figure 3.7: The schematic diagram of FTIR instrument (Jalvandi, 2016).

Meanwhile, Raman spectroscopy (Renishaw inVia Raman Microscope) with 512 nm wavelength laser source was used to characterize all the annealing and Argon plasma treated LB-rGO thin films. This characterization was conducted to investigate the vibrational, rotational and other stretching motion between sp^2 carbon atoms. Raman effect occurs when an incidental photon interacts on a molecule with its electric dipole. The arising scattering is described as an excitation of the molecules from ground state to an excited vibrational state. Thermal population of the molecular vibration excite at a very low rate at room temperature.

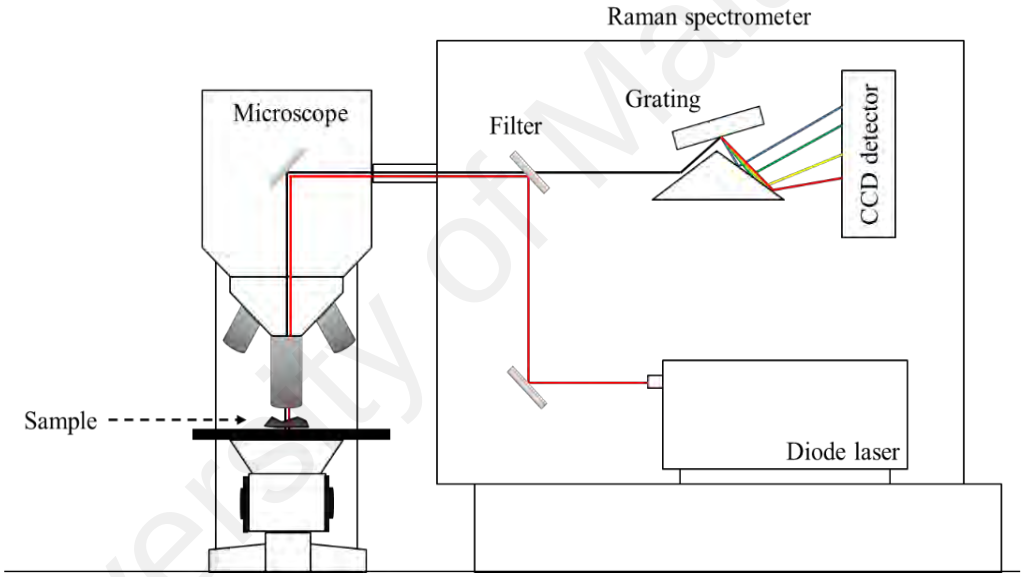

Figure 3.8: The schematic diagram of Raman spectroscopy.

As shown in Figure 3.8, the sample was exposed to a laser beam, and the electromagnetic radiation from the laser illumination point was captured with a lens and channeled through a monochromator. The Rayleigh scattering (elastic scattering) from the sample will react simultaneously to the incident laser beam while the rest of the scattered light will pass through a filter and get dispersed by the grating. A Raman shift commonly recognized in terms of wave number is reported as the units of inverse length, in relation to energy (Fenn et al., 2011).

In comparison to Raman spectroscopy, FTIR difference in certain significant aspects. For example, Raman spectroscopy depends on variation of molecular polarizability while FTIR spectroscopy tracks the dipole moment changes. Besides, Raman can characterize homo-nuclear molecular bonds such as C-C, C=C and C≡C bonds due to its sensitivity towards this type of bond. Meanwhile, FTIR spectroscopy is highly responsive to hetero-nuclear polar bonds and functional group vibrations, particularly OH stretching in water. On the other hand, Raman spectroscopy can obtain relative frequencies from the sample's scattered radiation. Unlike FTIR, it is capable of measuring absolute frequencies from sample absorbed radiation (Giusfredi et al., 2010).

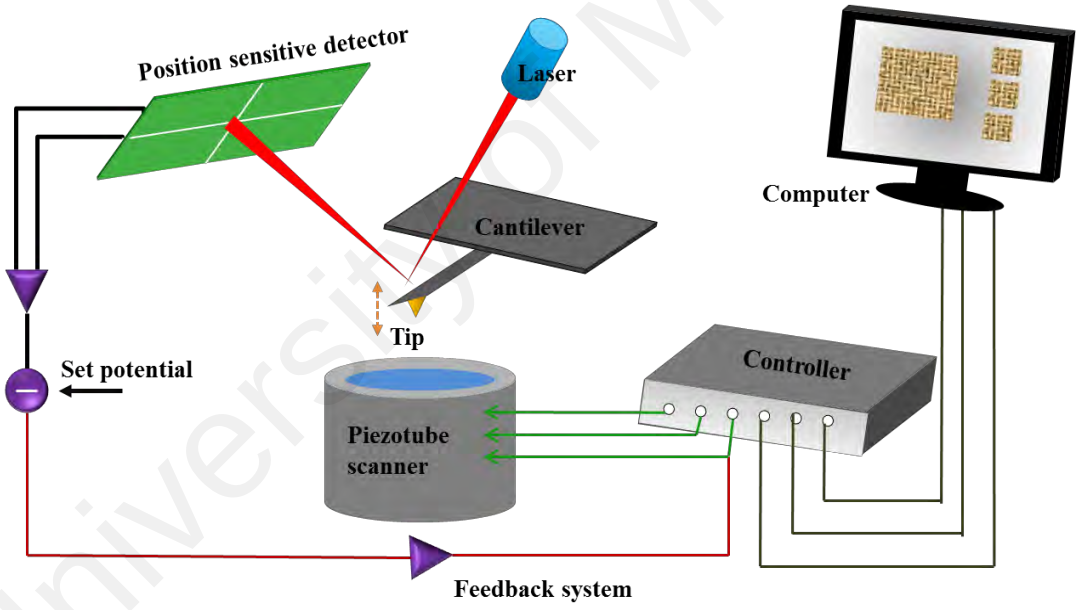

Figure 3.9: The schematic diagram of the basic working principle of AFM

Figure 3.9 shows the schematic diagram of the basic working principle of AFM (Guo et al., 2013). The sharp tip scans over the desired sample and the deflection of the AFM cantilever is computed through the beam of the laser that was reflected off the cantilever's backside to a photo detector. During scanning across the sample surface, the constant force maintained between the tip and the sample, giving rise to the deflection

of the tip instead allows the topographic image of the sample surface to be reproduced (Guo et al., 2013). In comparison to Scanning Electron Microscope (SEM), both AFM and SEM has complementary capabilities in order to visualize surface features. AFM characterization detailed out the features on basal planes and edges of the crystallites specifically on microvalleys, steps and ledge dimensions as well as crystallographic orientation of irregularities. In SEM images, the edges seemingly flattened and right-angled while in AFM images, the edges apparently leveled as a result of artifacts of the AFM tip dimensions. In addition, AFM manage to measure all three dimensions (x,y,z) with a single scan and is also known as a non-destructive sample characterization method compared to SEM (Zbik, 1998). Another characterization technique is used to investigate the crystalline phases in material, which is X-ray Diffraction Analysis (XRD). By investigating the crystalline phases, this technique could also be able to generate the information of chemical composition in material. Generally, most samples are finely ground to the form of powders before being analyzed using XRD.

CHAPTER 4: RESULTS AND DISCUSSION

4.1 Introduction

The structural, electrical and water contact angle of LB-rGO thin films were investigated thoroughly. This chapter also includes the results and its discussion of both the untreated and Argon plasma treated LB-rGO thin films and after the annealing treatment.

4.2 Characterization of Untreated LB-rGO Thin Films

4.2.1 Thickness and Sheet Resistivity

Table 4.1 shows the variation of the LB-rGO thin films thickness and the value of LB-rGO thin films sheet resistivity.

Table 4.1: Thickness and sheet resistivity due to the rGO deposition.

Deposition	Thickness reading (μm) ± 0.01	Sheet resistivity (Ω/sq)
1	0.57	1.66×10^6
2	1.03	3.34×10^5
3	1.28	1.83×10^5
4	1.82	1.16×10^5
5	2.05	9.16×10^4
6	2.59	7.83×10^4
7	2.91	6.48×10^4
8	3.70	5.43×10^4
9	4.67	5.23×10^4
10	5.06	4.41×10^4

In Figure 4.1, the graphs show that the values of sheet resistivity decrease due to the increasing LB-rGO thin film thickness. Sheet resistivity was observed to start saturating from the 6th layer of deposition until almost being parallel for the 10th layer. Therefore, 6 layers of rGO deposition was chosen as the number of layer for optimum thickness and resistivity to be used as the anode material in the BPV platform. The thickness and its relation to light transmittance are discussed in the following section.

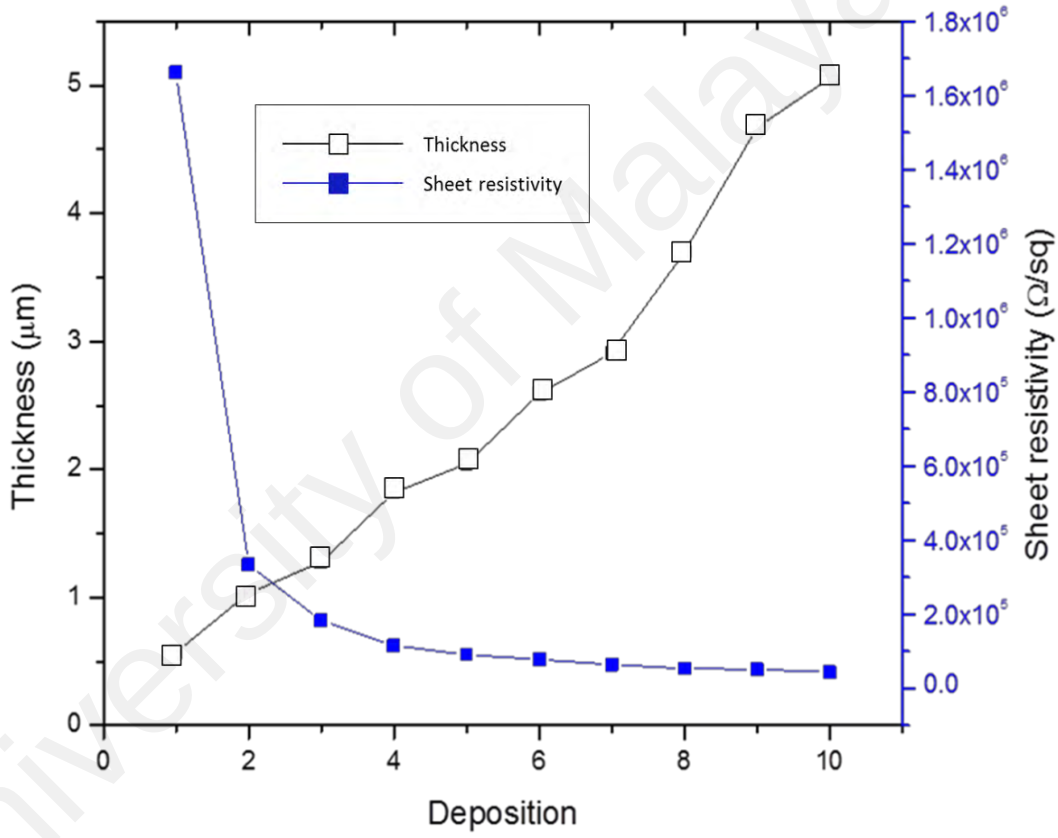

Figure 4.1: Graphs relating the influence of deposition, thickness and sheet resistivity.

4.2.2 Optical Properties

Figure 4.2 shows the percentage of transmittance based on the various layers of rGO deposition. One-layer deposition gives the highest transmittance percentage (60% at 300 nm) while ten layers' deposition gives the lowest transmittance percentage (~1% at 300 nm). This observation indicates that light hardly transmits through the 10

layers of deposition due to increased thickness. A cut-off between transmittance and resistivity, 6 layers of rGO deposition was therefore chosen for the application in our BPV experiments. Further, the algae will form a biofilm on top of the darker rGO layer, and as such will be freely exposed to light. Too thick of a layer as in ten layers of deposition, which may be more conductive (as indicated by the low resistivity value in Figure 4.1) however may not be suitable as this might make the surface of the layer more fragile and easily detachable from the substrate.

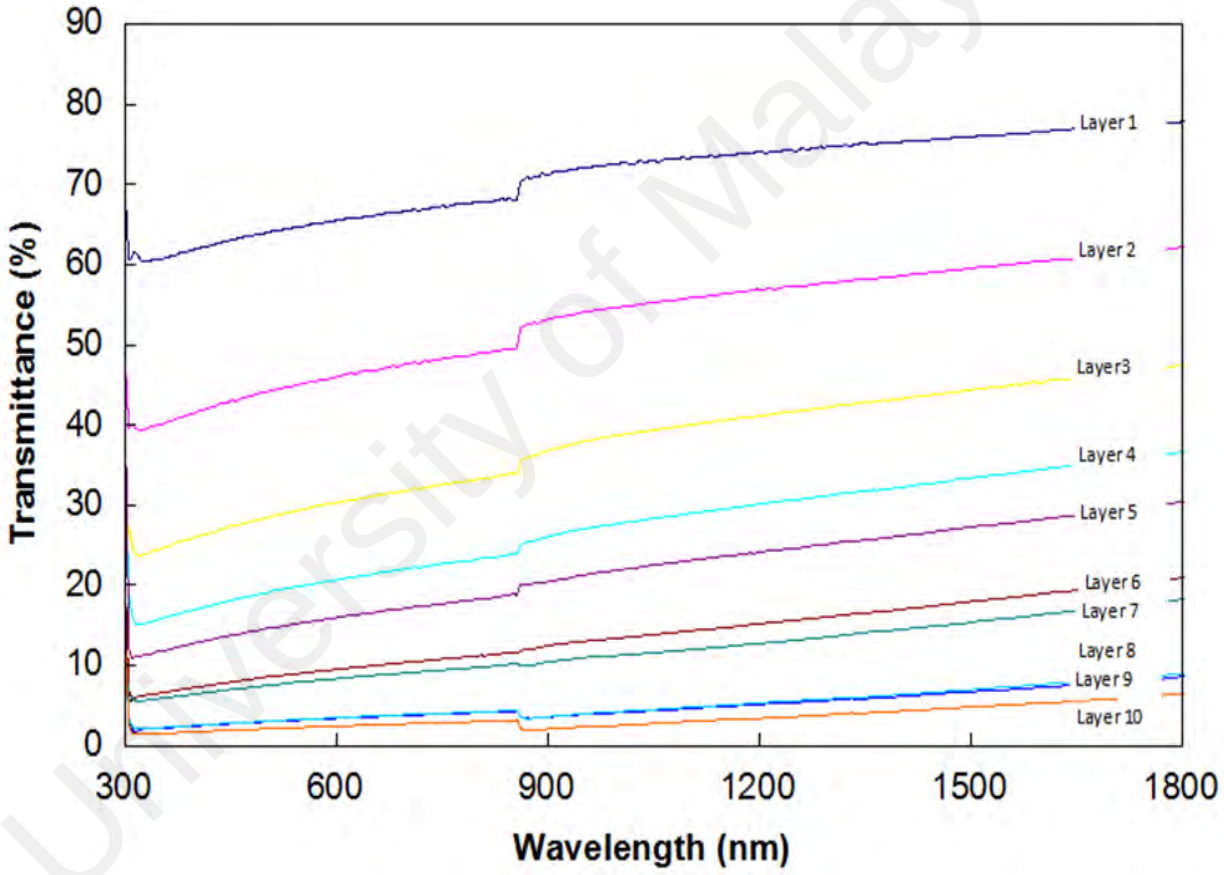

Figure 4.2: The optical transmittance graph with the indication of layer deposition.

4.2.3 Structural Properties

Figure 4.3 shows the FTIR spectra of non-treated LB-rGO thin film with 6 layers deposition. The chemical compound exhibited at 1558 cm^{-1} is due to the C=C stretching vibrations. The other spectra represent a strong absorption peak of C-O approximately at 893 cm^{-1} while at 762 cm^{-1} shows the existence of epoxy groups. This result for untreated rGO thin film will later be compared to the spectra obtained for treated ones (Section 4.3.4).

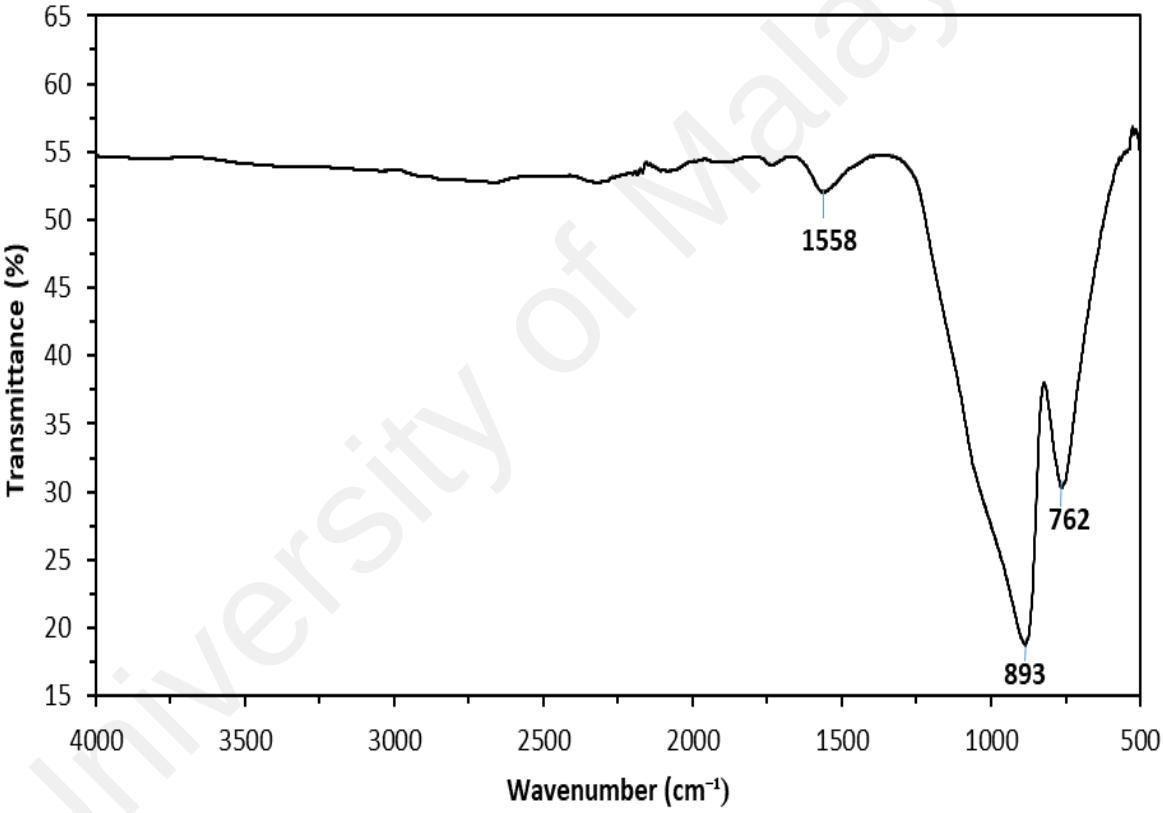

Figure 4.3: FTIR spectra for rGO thin film by LB deposition.

4.2.4 Contact Angle of LB-rGO Thin Films

Figure 4.4 below shows the water contact angle on non-treated LB-rGO thin film. The contact angle was calculated to be approximately 111.43˚. This value of contact angle indicates that the sample is a hydrophobic material by nature (Law, 2014). This

condition occurs due to the surface morphology of the untreated rGO sample. As such, this measurement can be carried-out to identify any changes in surface morphology of the sample after undergoing the treatment processes to be studied in this work (Section 4.3.2).

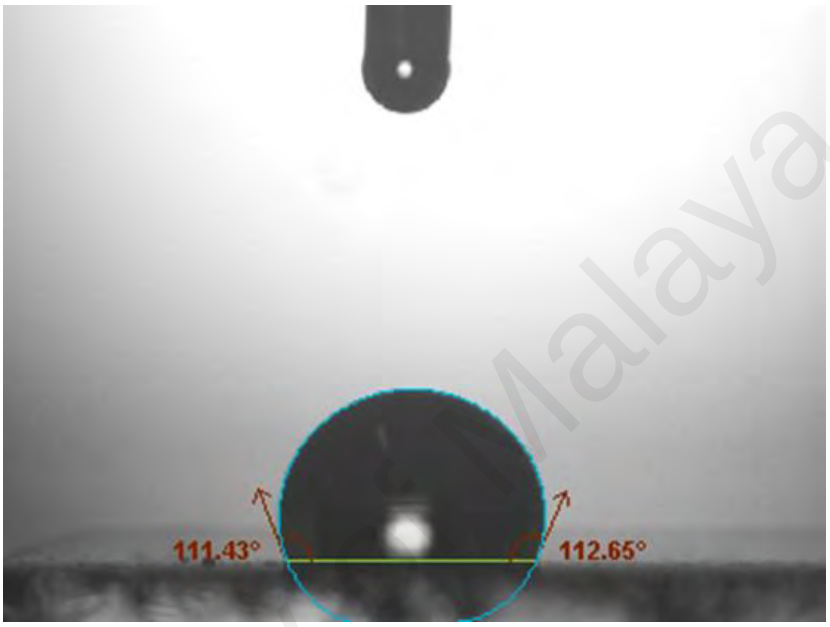

Figure 4.4: Water contact angle on non-treated LB-rGO thin film.

4.3 Characterization of LB-rGO Thin Films After Annealing and Plasma Treatment

4.3.1 Four-point Probe Measurement

Sheet resistance measurements are the conventional method of characterizing the homogeneity of conductive or semiconductive materials. Figure 4.5 shows the relation between sheet resistivity and annealing temperature of 6 layers of rGO films. As can be observed, the sheet resistivity was decreased as the temperature was increased. The highest sheet resistivity value of rGO film was 9.72×10^4 Ω/sq, while the lowest value was 3.47×10^4 Ω/sq at room temperature and 400 °C, respectively.

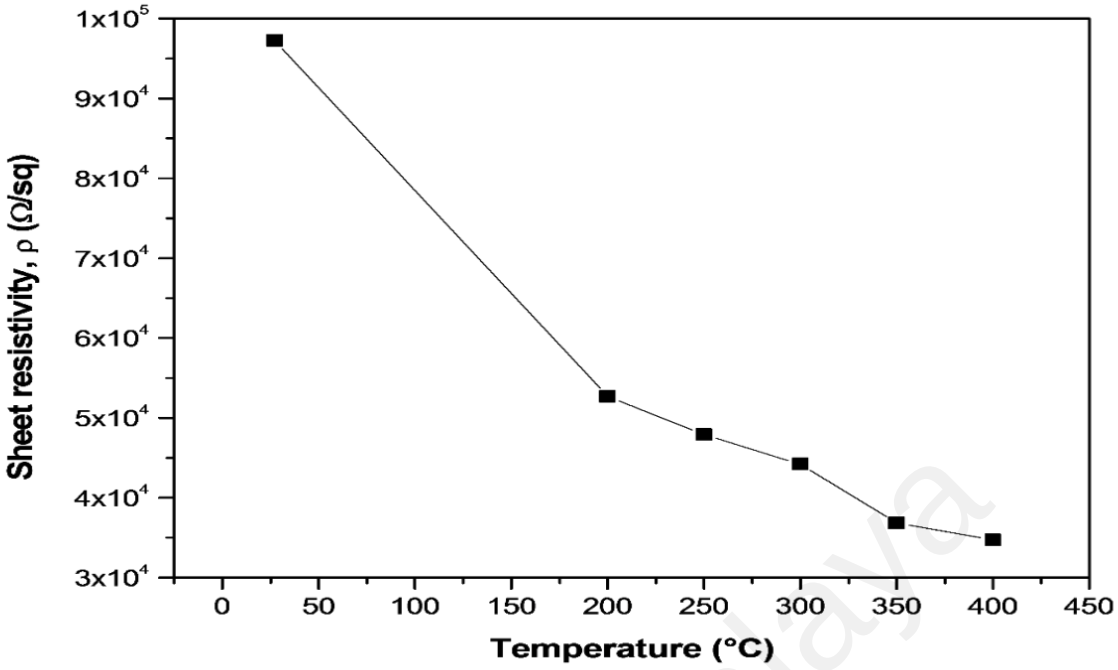

Figure 4.5: Sheet resistivity against temperature.

Figure 4.6 shows the graph of sheet resistivity versus plasma current for the rGO films. Based on Figure 4.6, the value of sheet resistivity increases due to increasing plasma power. The highest value of sheet resistivity of rGO film after plasma treatment was 6.84×10^5 Ω/sq, whereas the lowest value of sheet resistivity was 2.51×10^5 Ω/sq.

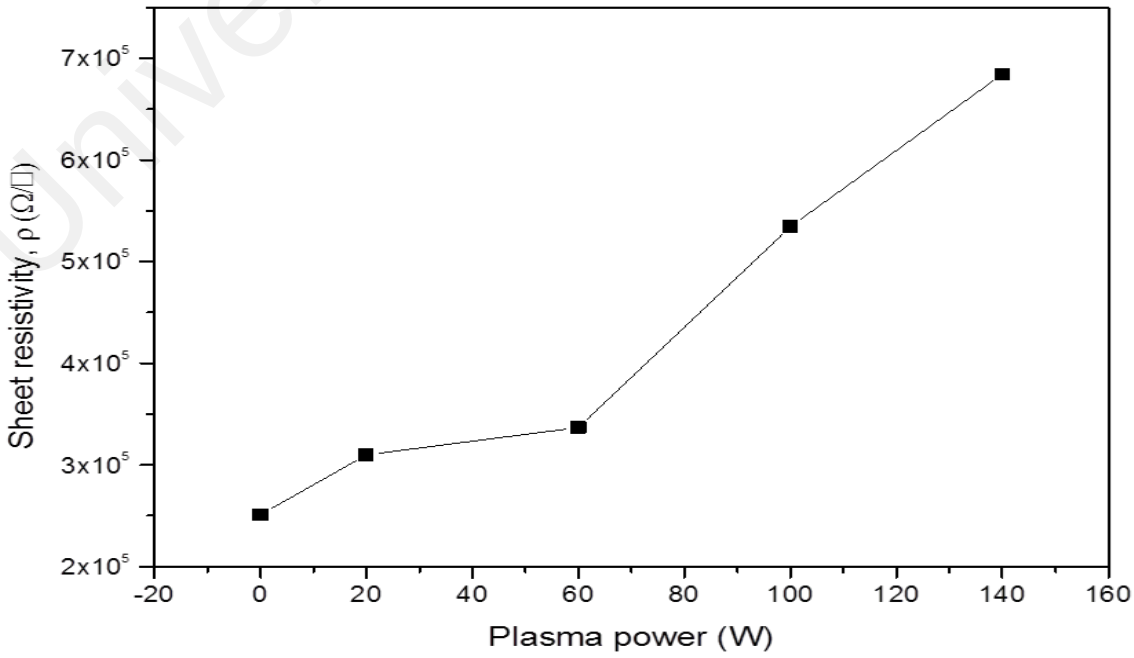

Figure 4.6: The graph of sheet resistivity against plasma power.

4.3.2 Water Contact Angle

The measurement of water contact angle is significant in understanding the thin films' surface properties. Figure 4.7 show the images of water contact angle on rGO films after the annealing treatment. At 350 °C, image clearly indicates an increment in hydrophilicity as the contact angle decreased. The highest and lowest values of contact angle were 118.01° and 86.45°, respectively.

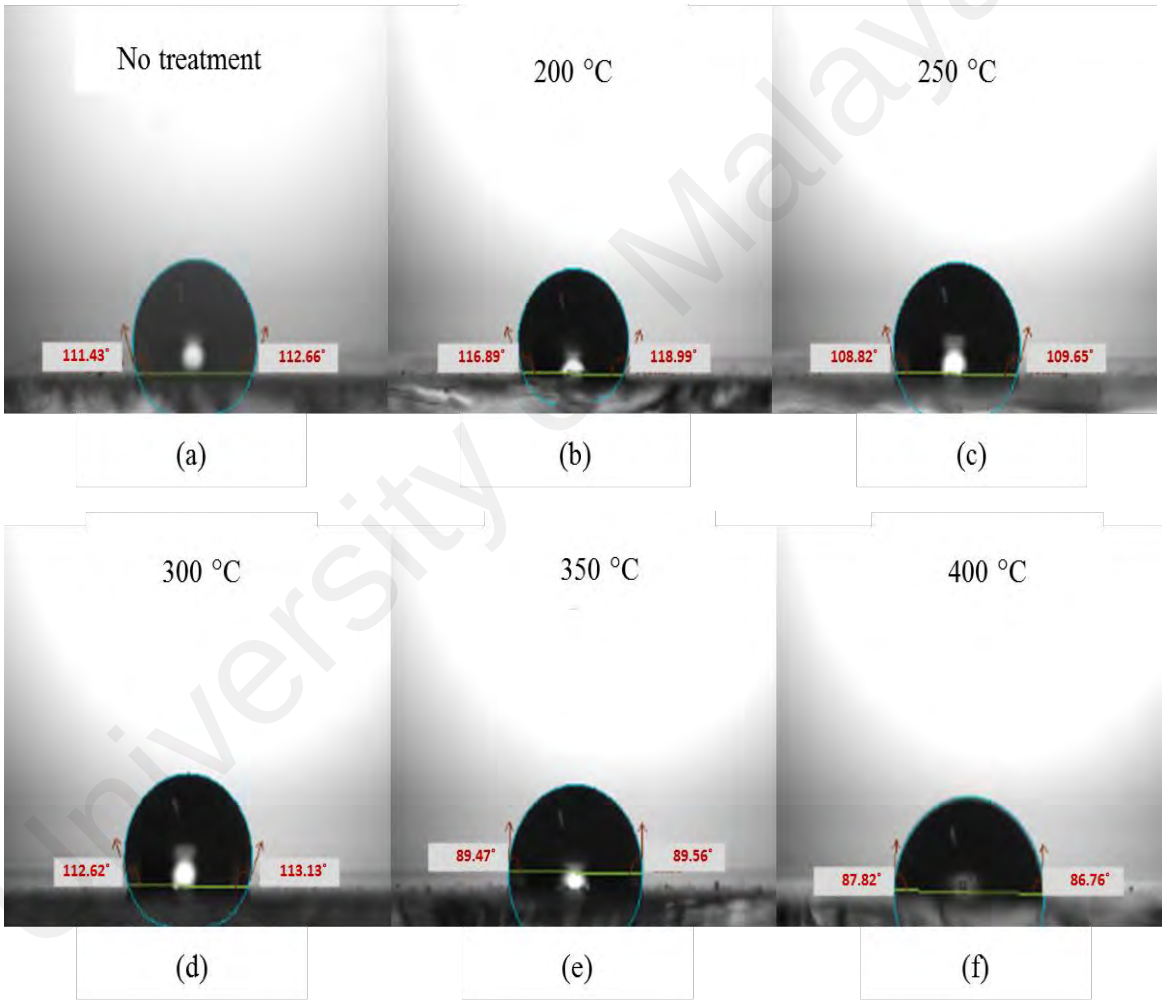

Figure 4.7: The images of water contact angle after annealed.

In order to interpret the possibility of modifying the wettability of the surface through surface morphology variation, contact angle measurements were tested. The value of contact angle for the untreated LB-rGO thin film was 69.15º. The contact angle

of LB-rGO thin film was obtained as 17.46º, 21.40º, 27.61º and 38.8º for 20, 60, 100 and 140 W of plasma treatment, respectively. The lowest contact angle value of 17.46º which is considered to be strongly hydrophilic was obtained from the 20 W of plasma treatment. Due to the increase in plasma power, the contact angle increased. At 140 W, the contact angle value was 38.8º, however it is still within the hydrophilic range. This trend of contact angle value indicates some modification of surface morphology and structural characteristics of the LB-rGO thin film occurring after the surface plasma treatment. The increase in roughness can be attributed to an increase of water contact angle due to the air content in the pores (Cassie et al., 1944).

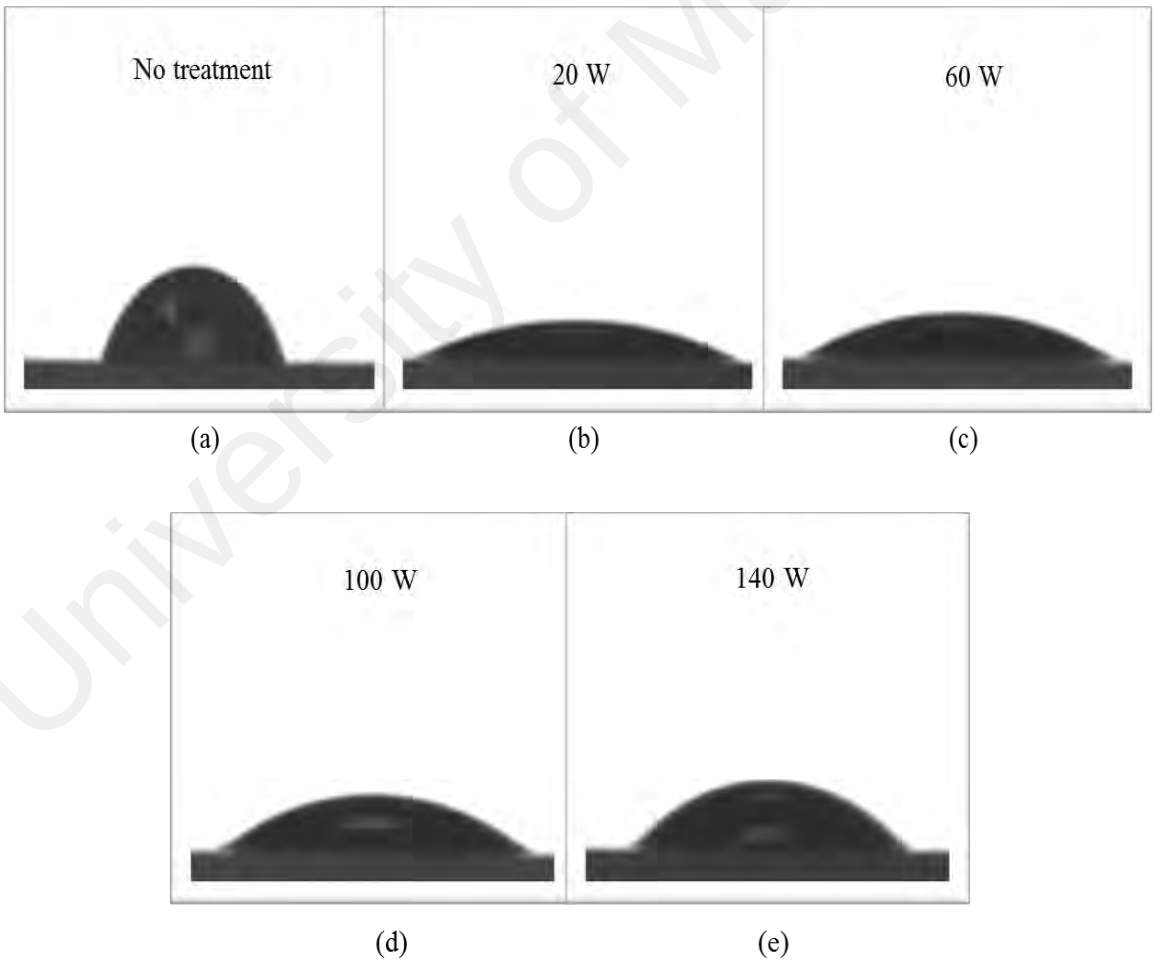

Figure 4.8: The image of water contact angle for each RF power of Argon plasma treatment.

4.3.3 Atomic Force Microscopy

AFM test was conducted to investigate the changes in surface roughness of untreated compared to that of the LB-rGO thin film treated with Argon plasma. Their AFM images are shown in Figure 4.9, which indicate the changes in surface roughness of the LB-rGO thin film and its dependence on the radio frequency (RF) power of the plasma. The treated sample does not appear to be smooth but it is to be noted that the sample treated with 20 W RF power has the lowest surface roughness of 0.131 μm. There was increment in surface roughness as the RF power of Argon plasma treatment increases, resulting in surface appearance of "hill-like" contour as can be seen in the AFM images of films treated with 60, 100 and 140 W.

The roughness was found to be 0.170 μm, 0.158 μm, 0.193 μm and 0.226 μm for untreated sample, 60 W, 100 W and 140 W, respectively. The increase in plasma power enhanced the bombardment energy of the Argon atom towards the surface area. These AFM images and surface roughness can be correlated with the wettability test results. Argon plasma treatment does not only change the roughness but has also increased the adhesion between the LB-rGO thin films with glass substrate. Normally, the enhancement of adhesion is related to the interfacial area formation between the underlying substrate and the film. As reported previously for thin film plasma deposition, the area covalently bonded to substrate by means of an interphase containing a cross-linked region (Liston et al., 1993).

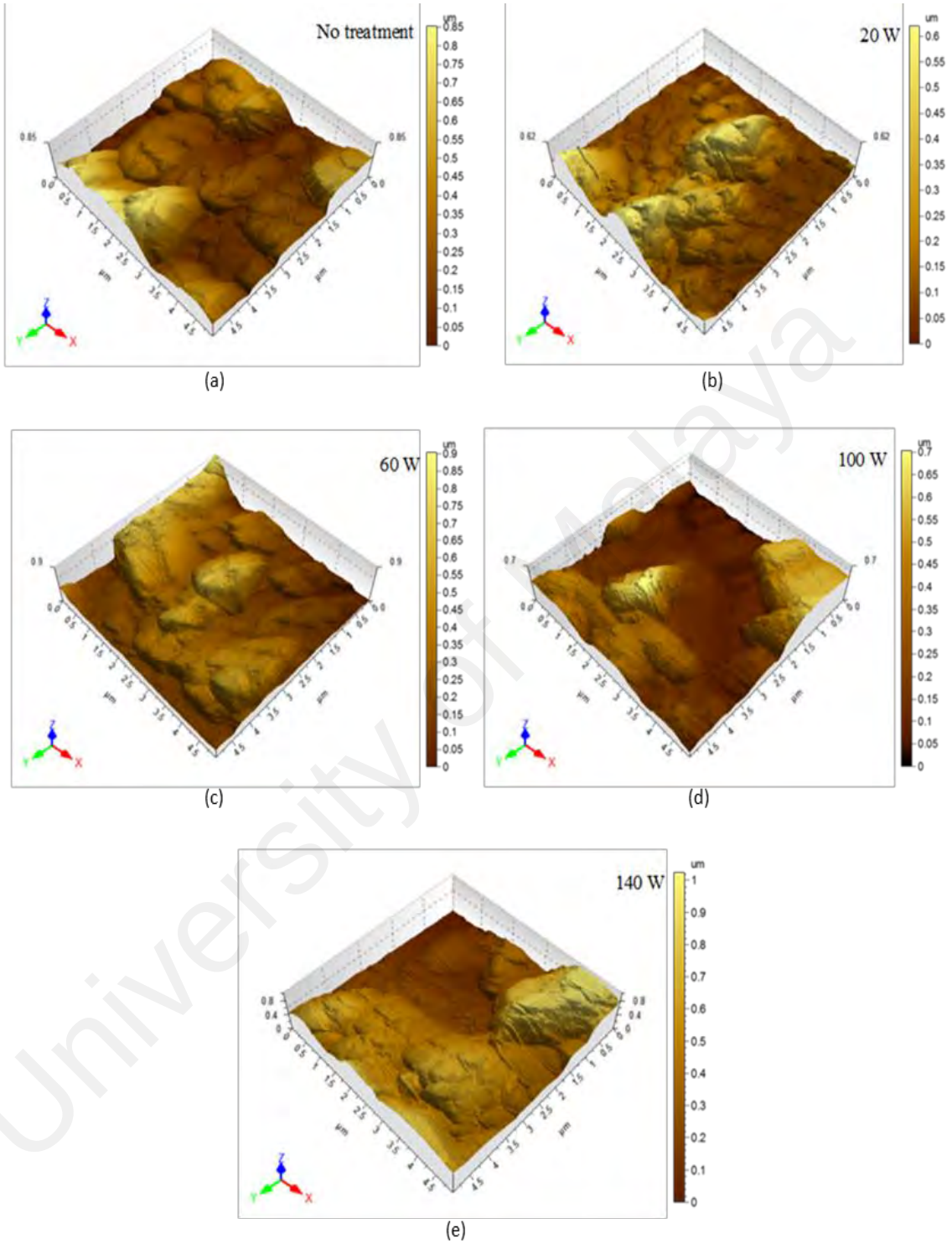

Figure 4.9: AFM image of rGO at different plasma power; (a) no treatment, (b) 20 W, (c) 60 W, (d) 100 W and (e) 140 W.

4.3.4 Fourier Transform Infrared Spectroscopy Analysis

FTIR characterization identifies chemical compounds and helps to understand the existence of functional groups in materials. The FTIR spectra were conducted to further characterize the functionalization of LB-rGO after plasma treatment. Absorption peaks due to the C=O, C=C and C–O stretching vibration appeared approximately at 1750 cm^{-1}, 1550 cm^{-1} and 915.87 cm^{-1}. The characteristic bands approximately at 786 cm^{-1} confirm the presence of the epoxy groups corresponding to the deformation vibrations and asymmetric stretching. Furthermore, the broad absorption band due to the presence of O–H stretching vibration is observed around 3475 cm^{-1} while untreated rGO spectra shows narrow band at the similar wavenumber range.

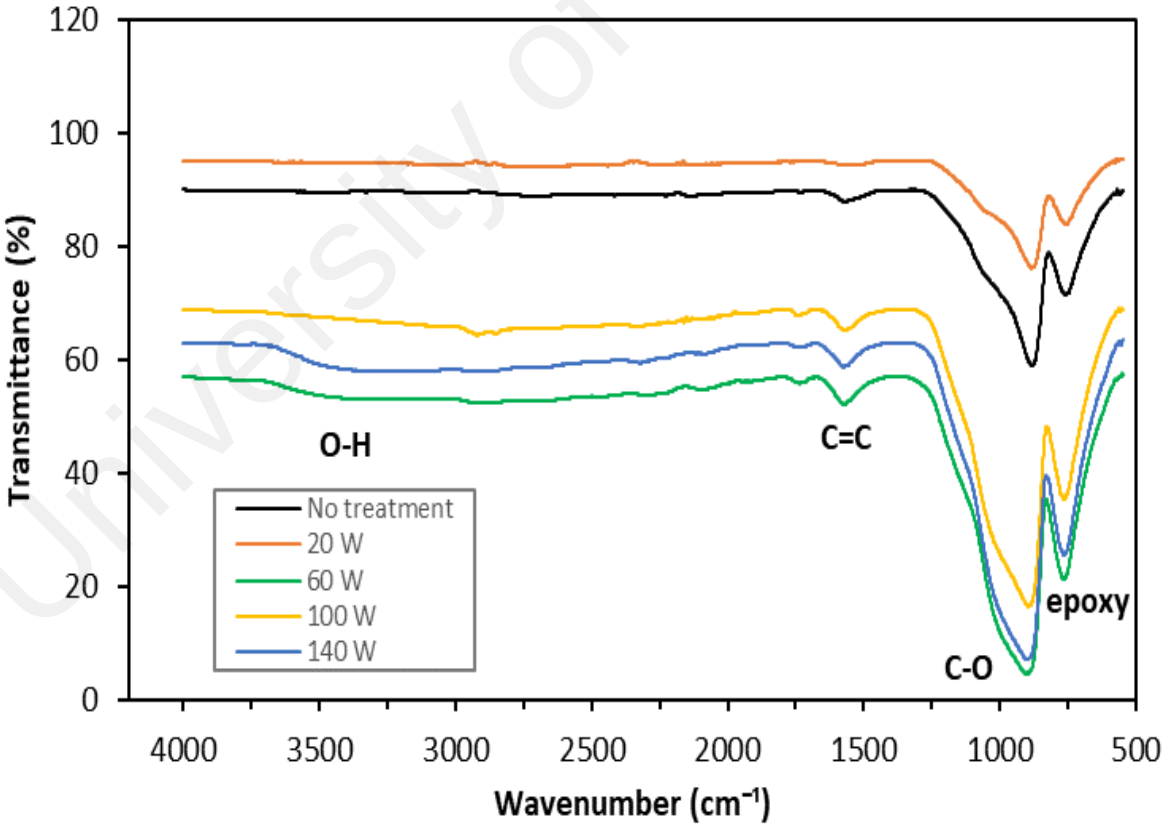

Figure 4.10: FTIR image of LB-rGO after Argon plasma treatment.

4.3.5 Raman Spectroscopy

Figures 4.11 and 4.12 shows the image of Raman spectrum for LB-rGO thin film after annealing and Argon plasma treatment. In carbon materials, the D and G peaks are dominant. The D peak represents disordered bond originating from the structural defects and edge effects, while the G peak appears due to the presence of stretching motion between sp2 carbon atoms. For the D peak, the significant value of wavenumber for graphene and GO is 1344 cm^{-1} and 1351 cm^{-1}, respectively whereas the G peak was 1576 cm^{-1} and 1593 cm^{-1}, respectively. The Raman peaks show changes in band position and shape during the oxidation reaction. The value of integrated intensity ratio of D and G band (I_D/I_G) of GO is higher than pristine graphite. This phenomenon indicates that the oxidation of graphite has occurred. In addition, the I_D/I_G ratio is decreased during the reduction of GO confirming the de-functionalization of hydroxyl, epoxide as well as the other functional groups of oxygen.

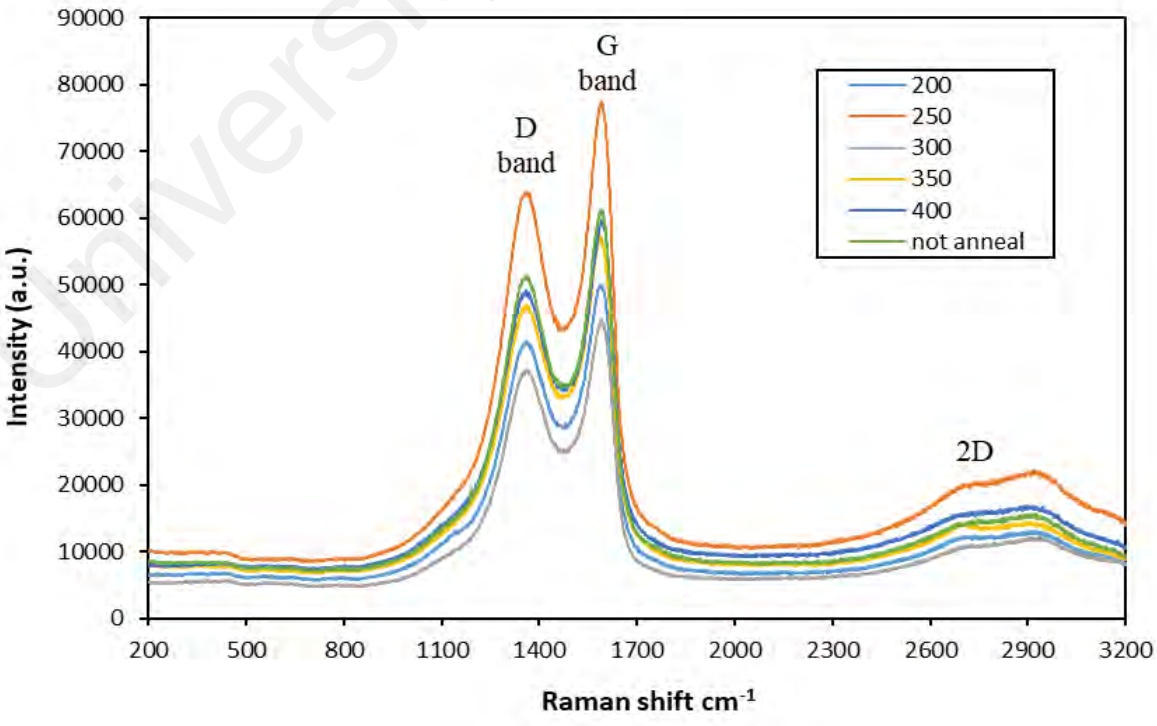

Figure 4.11: Raman spectrum for LB-rGO thin film after the annealing treatment.

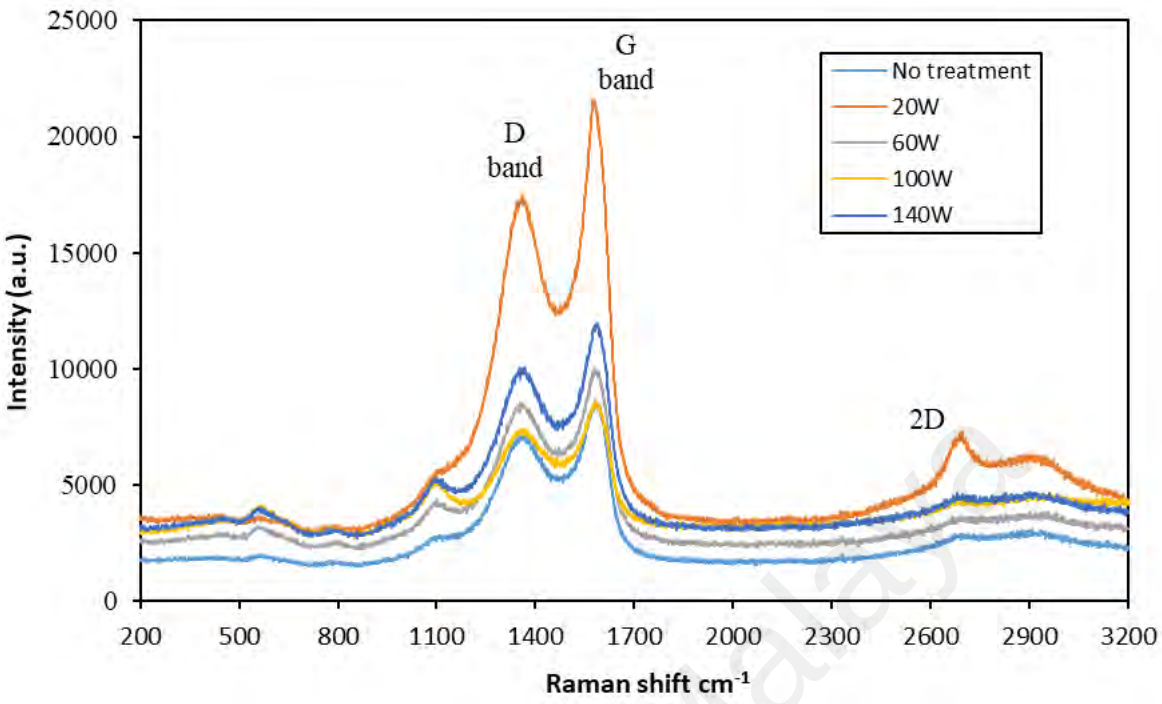

Figure 4.12: Raman spectrum for LB-rGO thin film after Argon plasma treatment.

Tables 4.2 and 4.3 lists the I_D/I_G value of LB-rGO thin film after annealing and Argon plasma treatment. The first table shows that the value of I_D/I_G of LB-rGO thin film after annealing treatment gradually decrease due to the increasing of temperature. Table 4.3 meanwhile demonstrates that the trend of I_D/I_G for LB-rGO thin film after Argon plasma treatment is slightly different where the values are observed to decrease until 100 W but increase at 140 W.

Table 4.2: (I_D/I_G) of LB-rGO thin film after annealing treatment.

No.	Temperature (°C)	$I_D/I_G \pm 0.01$
1.	Non-annealed	0.84
2.	200	0.83
3.	250	0.83
4.	300	0.83
5.	350	0.82
6.	400	0.82

Table 4.3: (I_D/I_G) of LB-rGO thin film after Argon plasma treatment.

No.	Plasma Power (Watts)	$I_D/I_G \pm 0.01$
1.	Non-treated	0.83
2.	20	0.81
3.	60	0.77
4.	100	0.82
5.	140	0.84

4.3.6 Chlorophyll Extraction

Tables 4.4 and 4.5 show the extraction of Chlorophyll-a (Chl-a) concentration from the *Chlorella* sp. (UMACC 313) biofilm grown on the treated LB-rGO thin film. As can be seen in Table 4.4, the highest concentration of Chl-a extraction yield is 4.41 ± 0.02 mg/L while in Table 4.5, the highest value of concentration is 4.42 ± 0.04 mg/L. These values of concentration represent the sample treated at 250 ˚C and 100 W accordingly.

Table 4.4: Chlorophyll extraction for annealing treatment.

Temperature (°C)	Chl-a (mg/L)
NA	1.51 ± 0.03
200	1.14 ± 0.01
250	4.41 ± 0.02
300	3.84 ± 0.02
350	1.87 ± 0.01
400	2.08 ± 0.02

Table 4.5: Chlorophyll extraction for Argon plasma treatment.

Plasma Power (Watts)	Chl-a (mg/L)
NA	1.53 ± 0.03
20	1.19 ± 0.02
60	4.16 ± 0.28
100	4.42 ± 0.04
140	1.55 ± 4.64

Chlorophyll is the pigment found in majority of plants that reflects green color. This pigment functions to harness the light for the photosynthesis activity. Chlorophyll is divided into two types; Chl-a and Chl-b. They have slight difference in one small composition side chain where Chl-a consists of $-CH_3$ while -CHO is found in Chl-b. The growth of the algal cells can be indicated by the concentration of Chlorophyll a (Chl-a). Chlorophytes *Chlorella vulgaris* (UMACC 051) and *Chlorella* sp. (UMACC 313), and the Cyanophytes *Synechoccus elongatus* (UMACC 105) and *Spirulina platensis* (UMACC 159) are the examples of the strains that able to generate the output of the electrical power. Meanwhile, *Synechococcus elongatus* (UMACC105) and Chlorella (UMACC 313) are reported to be the best candidates in forming substantial biofilm where it only takes three days to form. This may be the results of the extra-cellular polymeric substances (EPS) high production of *Synechococcus elongatus* (UMACC105) and the *Chlorella* (UMACC 313) high growth rate (Ng et al., 2014b).

4.4 Polarization Curve for Annealed and Plasma Treated rGO-based BPV Device

4.4.1 Annealed Treated LB rGO Thin Films

Figures 4.13 to 4.18 represent the polarization curves of non- annealed LB-rGO thin film, 200 ˚C, 250 ˚C, 300 ˚C, 350 ˚C and 400 ˚C treated LB-rGO thin films. Figure 4.13 shows the polarization curve of the non-annealed LB-rGO thin film. In light condition, the highest power density was (74.1 ± 7.7) $\mu W/m^2$ while in the dark the highest power density was 43.8 ± 0.1 $\mu W/m^2$. Polarization curve of the LB-rGO thin film prepared after annealing at 200 °C temperature meanwhile is shown in Figure 4.14. Sample prepared at this temperature shows highest power density of 15.9 ± 0.4 $\mu W/m^2$ and 19.8 ± 0.4 $\mu W/m^2$ at light and dark conditions, respectively.

At higher temperatures of annealing, polarization curve of LB-rGO thin film at 250 °C temperature (Figure 4.15) results in the highest power density of 97.7 ± 9.8 $\mu W/m^2$ during the light condition. At the same temperature, the highest power density measured in the dark was of 67.3 ± 0.5 $\mu W/m^2$. These values correspond to 66.6 ± 7.2 $\mu W/m^2$ and 43.6 ± 0.3 $\mu W/m^2$ for light and dark conditions, respectively when the annealing temperature was 300 °C (Figure 4.16). For 350 °C and 400 °C, the values were 166.0 ± 32.0 $\mu W/m^2$, 123.0 ± 14.0 $\mu W/m^2$ and were 211.0 ± 1.0 $\mu W/m^2$, 157.0 ± 1.0 $\mu W/m^2$, respectively for light and dark conditions (Figures 4.17 – 4.18).

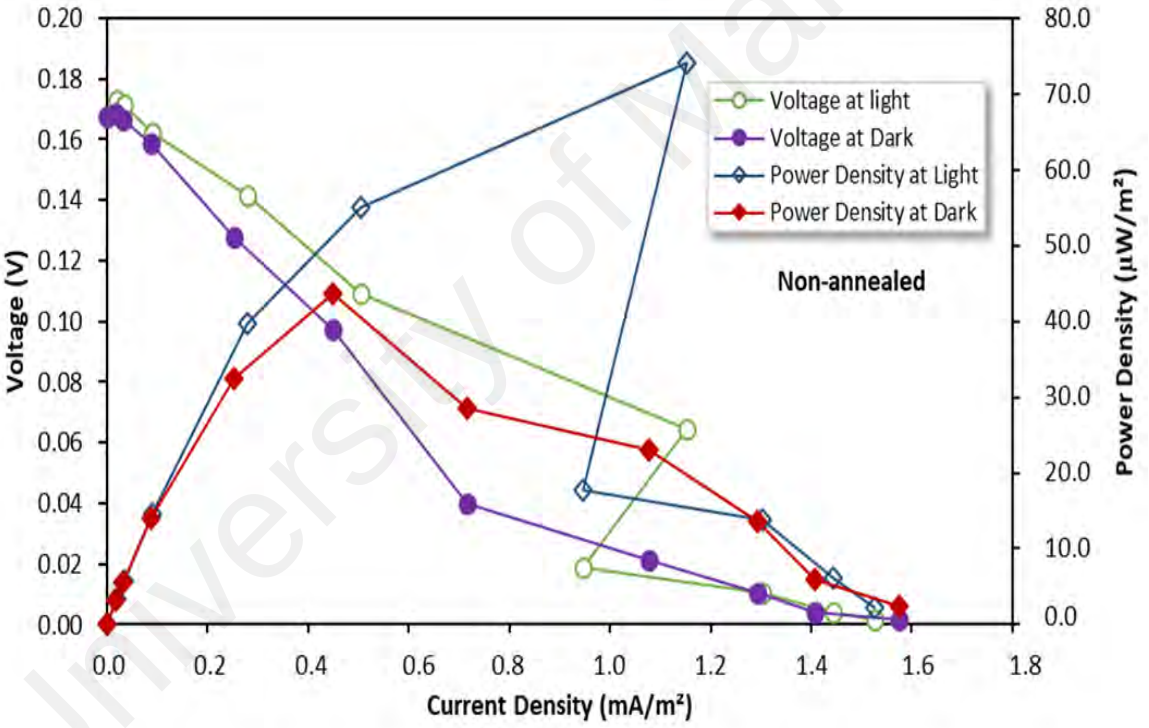

Figure 4.13: Polarization curve of non-annealed LB-rGO thin films.

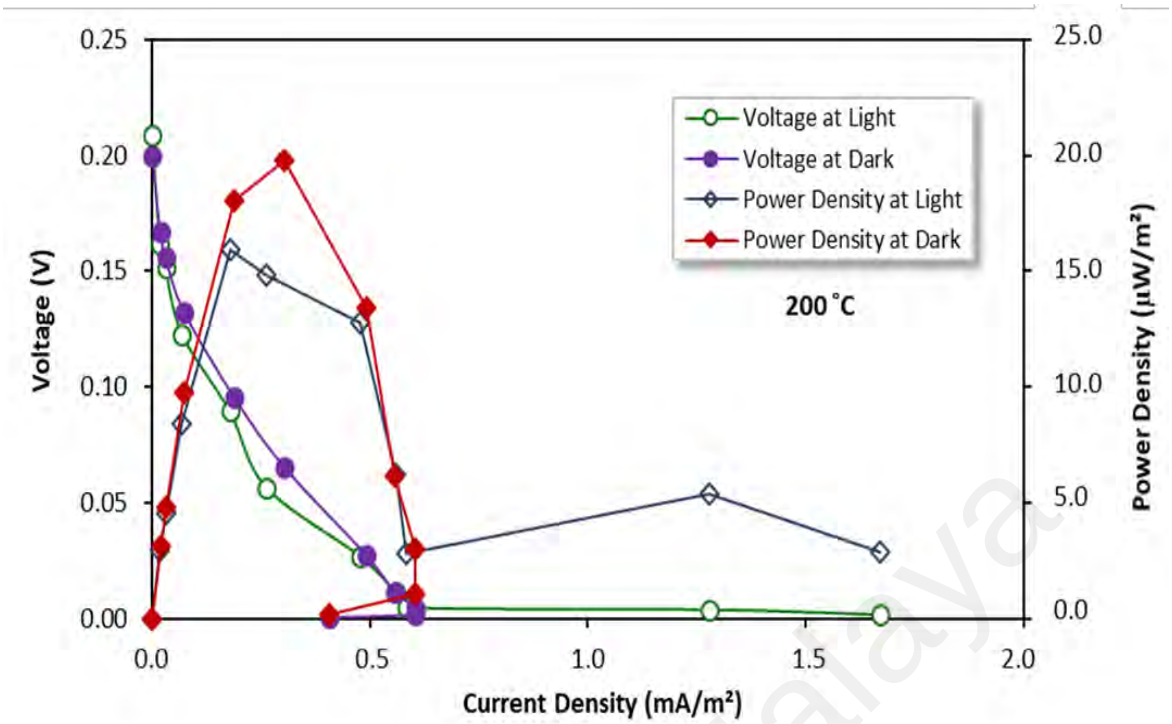

Figure 4.14: Polarization curve of 200 ˚C treated LB-rGO thin films.

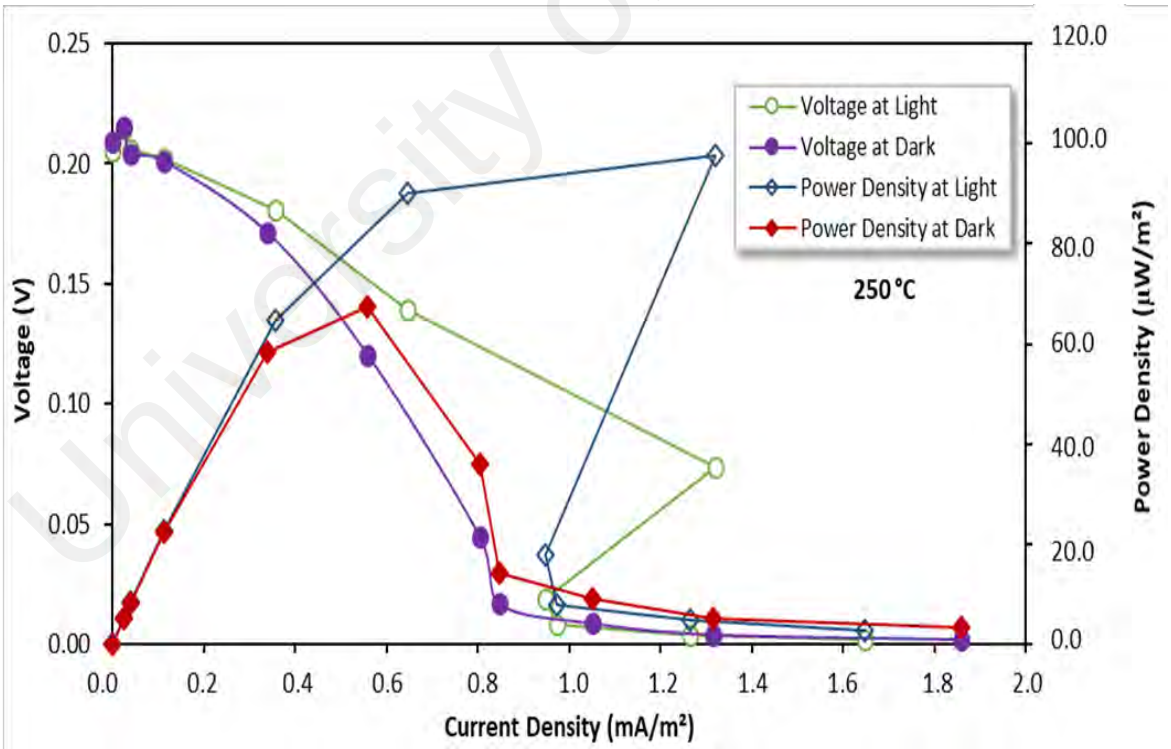

Figure 4.15: Polarization curve of 250 ˚C treated LB-rGO thin films.

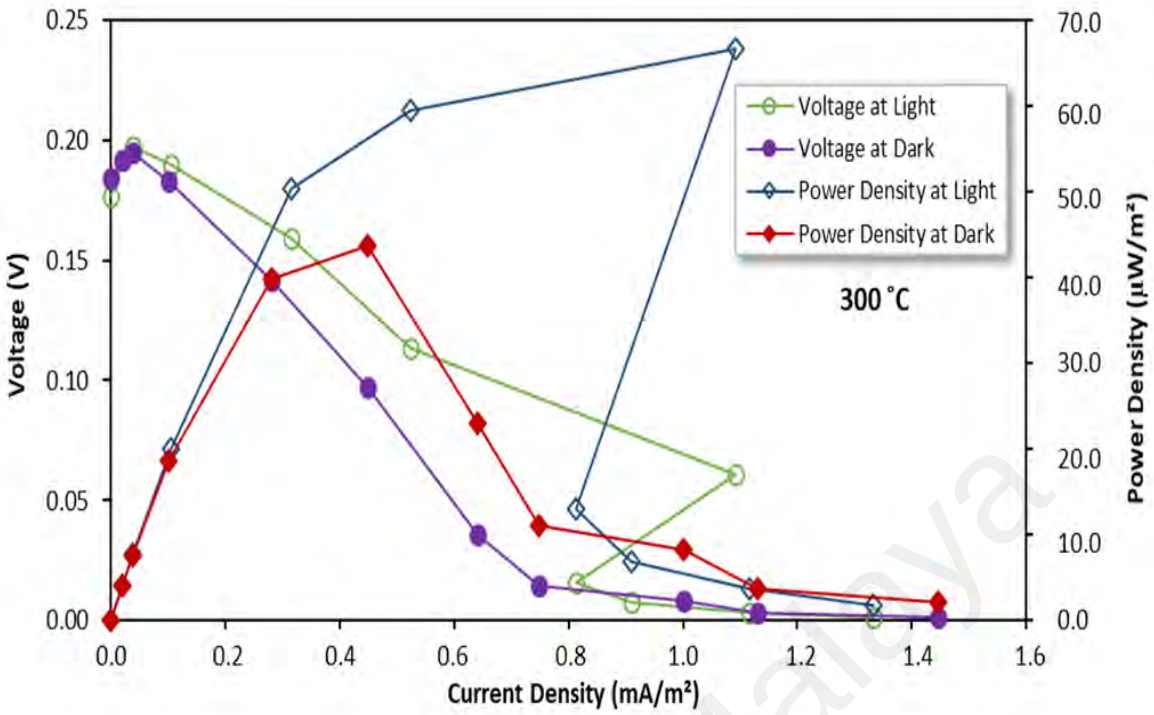

Figure 4.16: Polarization curve of 300 ˚C treated LB-rGO thin films.

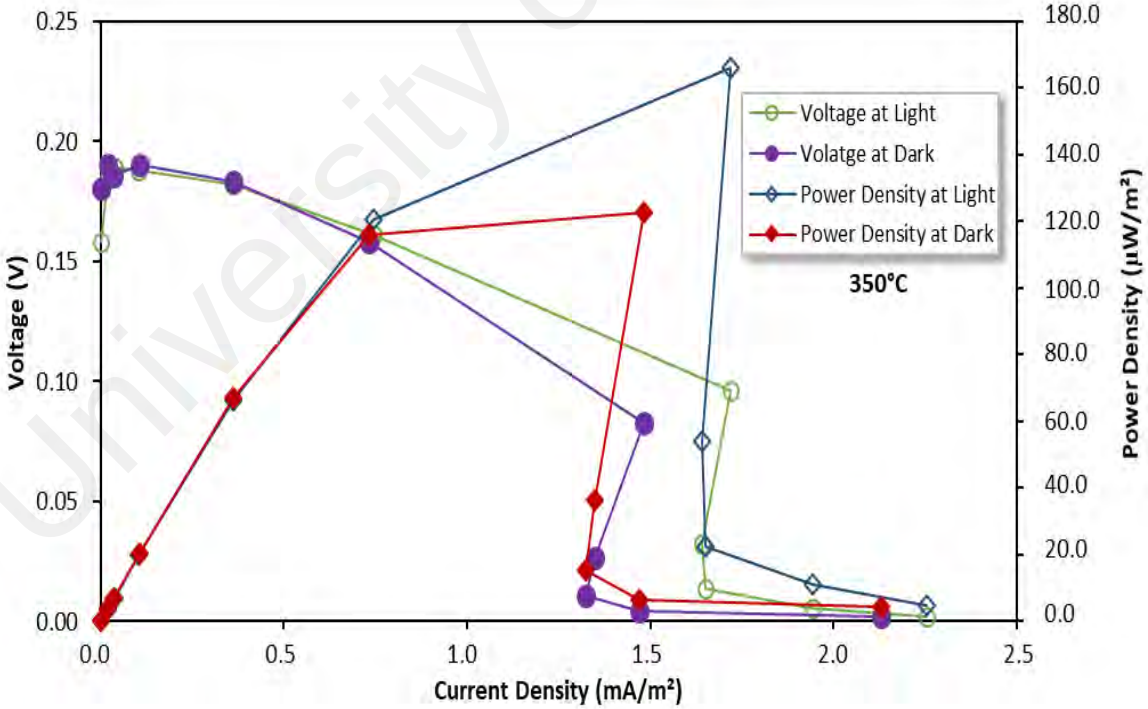

Figure 4.17: Polarization curve of 350 ˚C treated LB-rGO thin films.

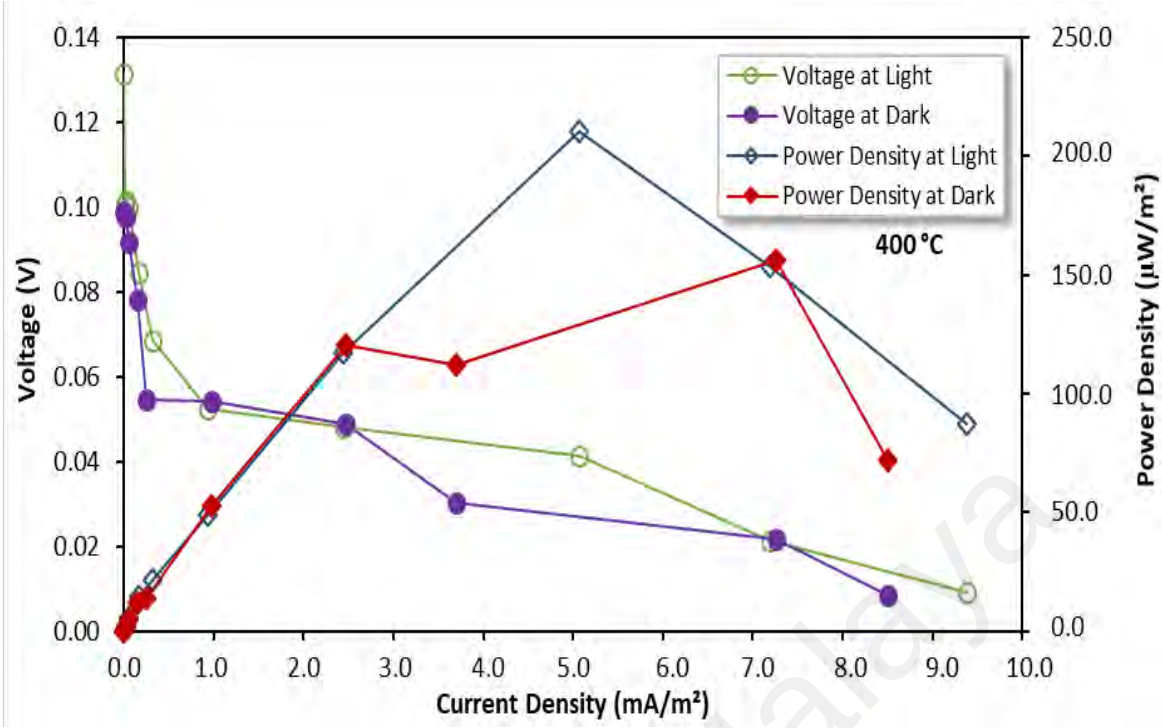

Figure 4.18: Polarization curve of 400 ˚C treated LB-rGO thin films.

From direct comparison graph of maximum power density for LB-rGO thin films in Figure 4.19, highest power density in light condition was 211.0 ± 1.0 μW/m^2, while in dark condition it was 157.0 ± 1.0 μW/m^2 in 400 °C rGO thin films. The lowest power density meanwhile was 1.13 ± 0.11 μW/m^2 and 1.06 ± 0.06 μW/m^2 in light and dark conditions, respectively. We observe here power density was higher in dark compared to light condition for LB-rGO thin films annealed at 200 °C whereas higher values were observed in light condition for 250 °C, 300 °C, 350 °C and 400 °C. One explanation may be contributed to redox processes occurring within the algae cells during "night" or in the absence of light. In dark condition, algae may produce electrons generated from redox-related metabolic processes and respiration. Based on the current response that had been observed in both light and dark condition, the electrons were possibly generated from both photosynthetic electron transport chain (PETC) and respiratory electron transport chain (RETC). In addition, the power output under dark condition is in relation to chlorophyll concentration (Tschörtner et al., 2019).

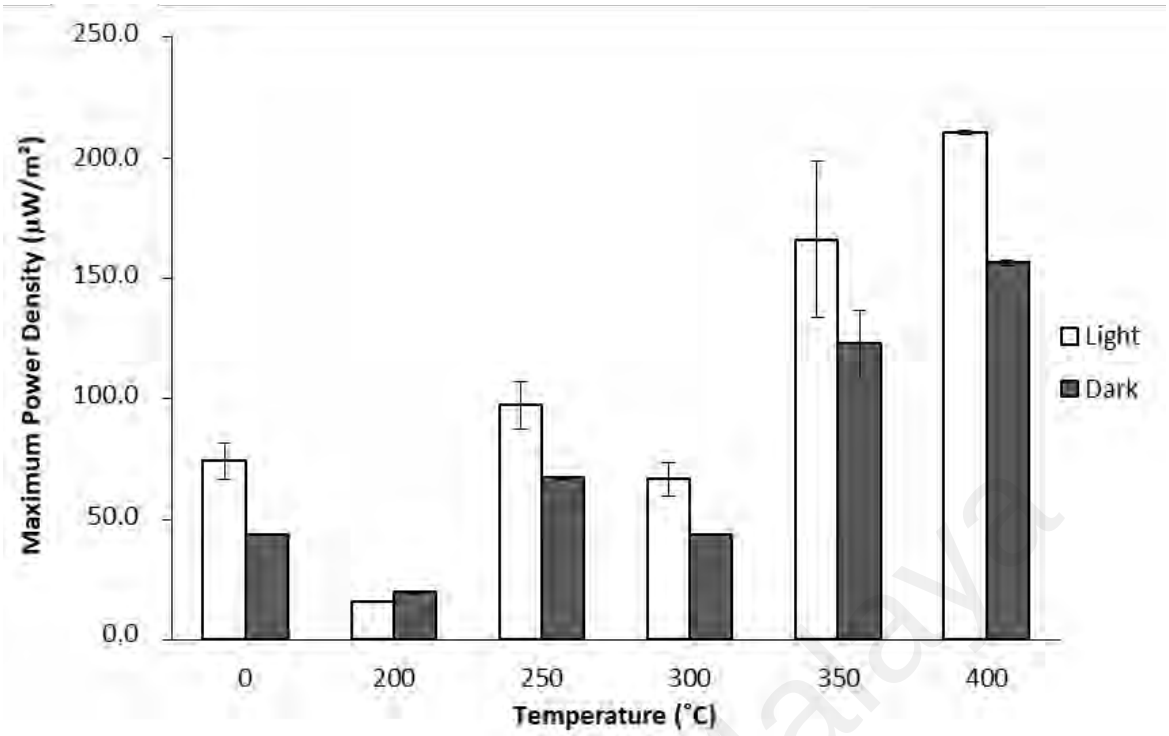

Figure 4.19: Direct comparison of maximum power density for annealing treated LB-rGO thin films.

4.4.2 Plasma Treated LB rGO Thin Films

Figure 4.20 to 4.24 shows the polarization curve of non-treated Argon plasma LB-rGO thin film, 20 W, 60 W, 100 W and 140 W Argon plasma treated LB-rGO thin films. The highest power density calculated was 36.7 ± 2.1) $\mu W/m^2$, 37.9 ± 2.5) $\mu W/m^2$, 30.8 ± 0.7 $\mu W/m^2$, 69.3 ± 0.9) $\mu W/m^2$ and 28.9 ± 0.03 $\mu W/m^2$ in light condition for non-treated (0 W), 20 W, 60 W, 100 W and 140 W, respectively. In dark condition, these values corresponded to be 35.0 ± 0.3 $\mu W/m^2$, 44.5 ± 4.4 $\mu W/m^2$, 35.1 ± 0.4 $\mu W/m^2$, 28.4 ± 0.2 $\mu W/m^2$ and 18.9 ± 0.1 $\mu W/m^2$, respectively for the same range of plasma power.

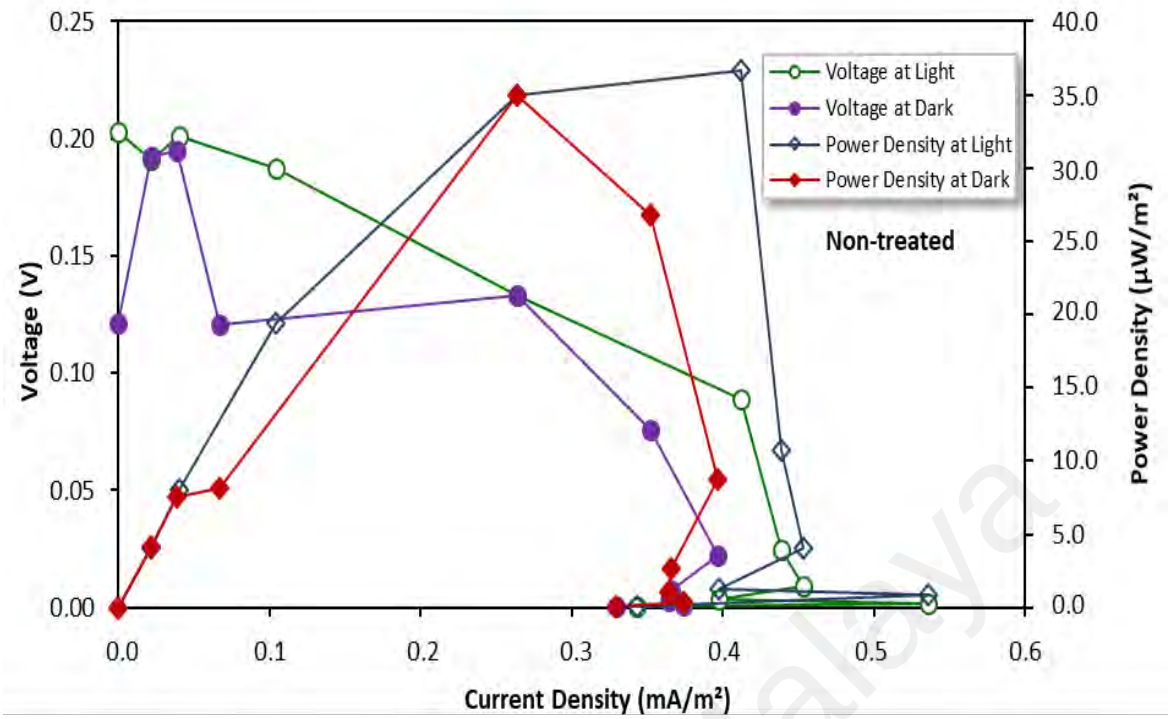

Figure 4.20: Polarization curve of non-treated LB-rGO thin films.

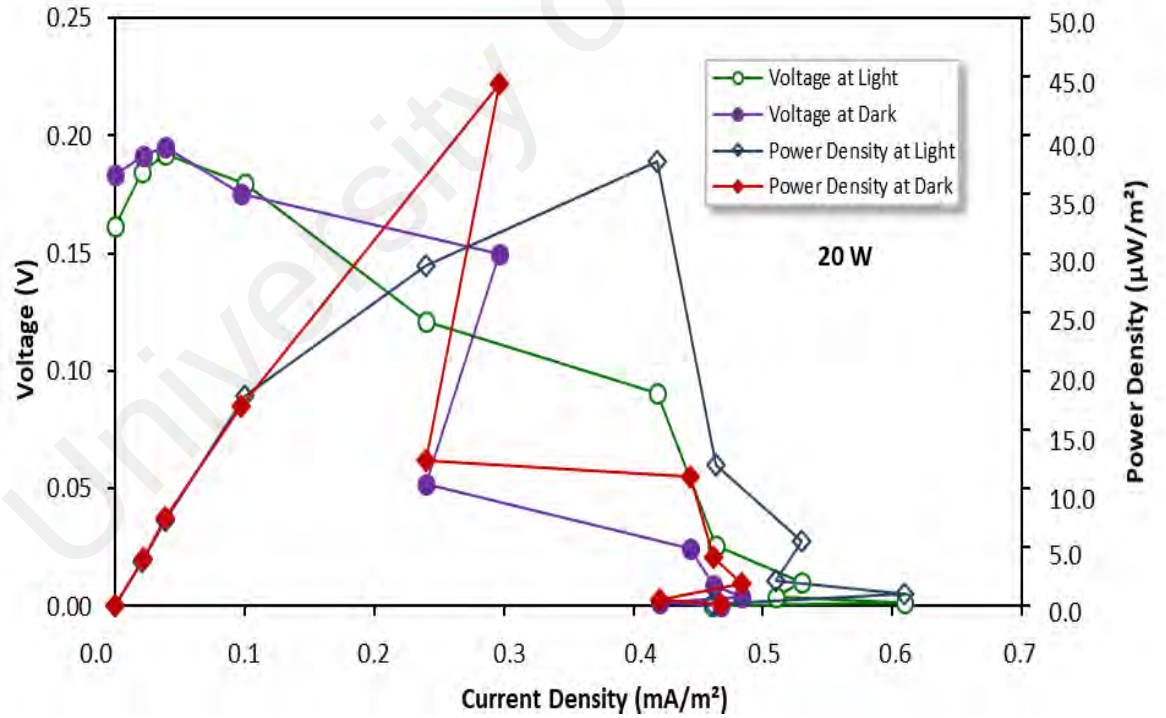

Figure 4.21: Polarization curve of Argon plasma treated LB-rGO thin films at 20 W.

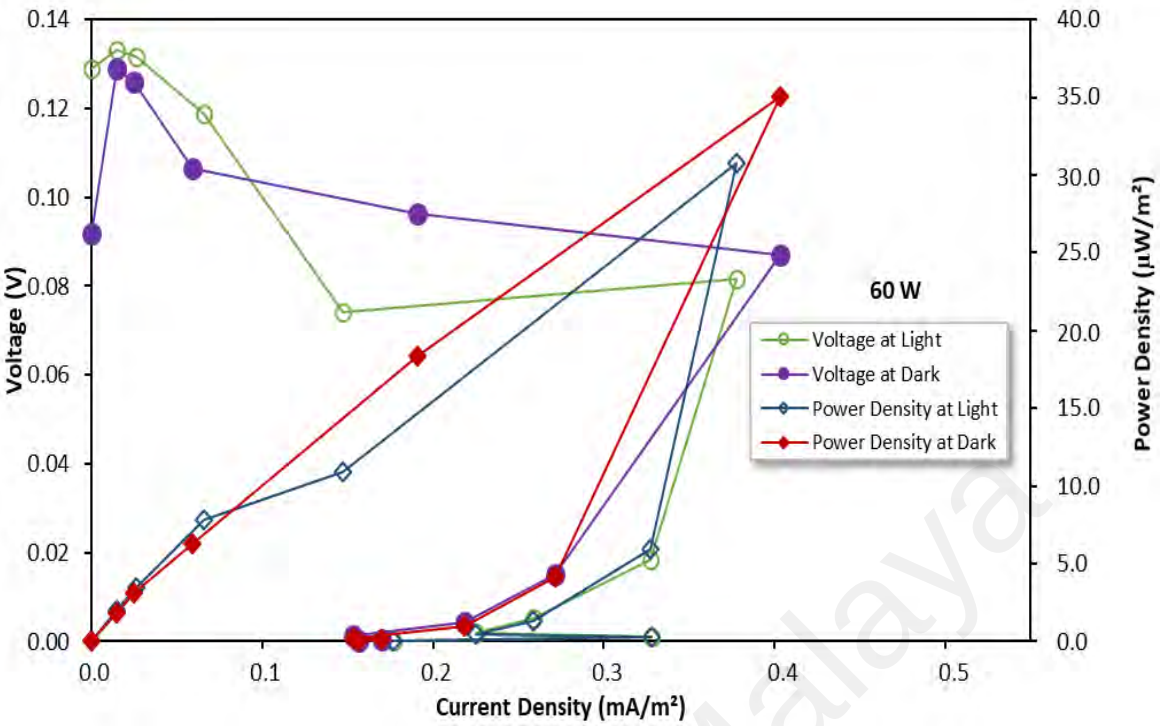

Figure 4.22: Polarization curve of Argon plasma treated LB-rGO thin films at 60 W.

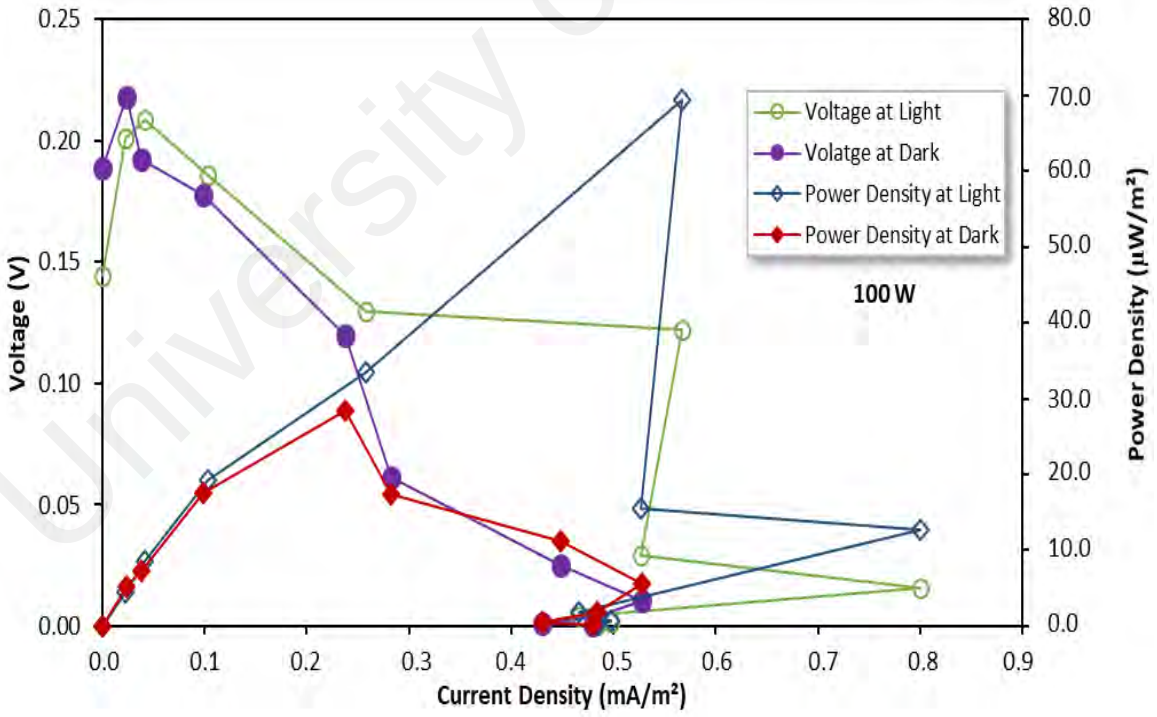

Figure 4.23: Polarization curve of Argon plasma treated LB-rGO thin films at 100 W.

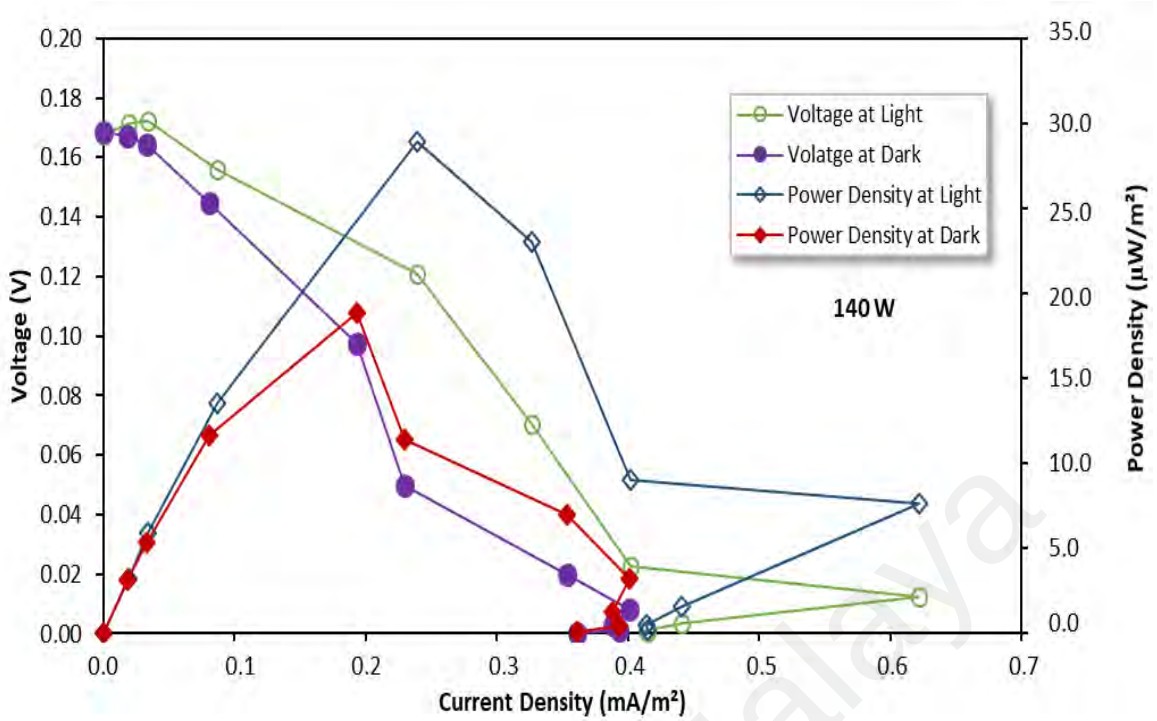

Figure 4.24: Polarization curve of Argon plasma treated LB-rGO thin films at 140 W.

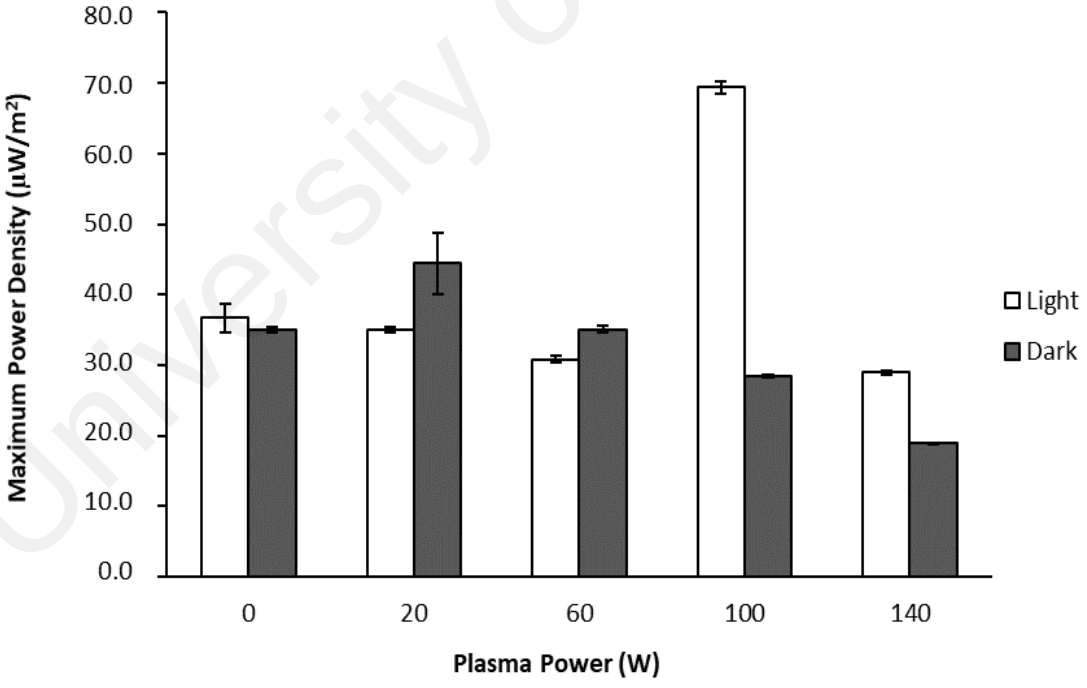

Figure 4.25: Direct comparison of maximum power density of plasma power for LB-rGO thin films.

In summary, the direct comparison of maximum power density graph shows that the highest power density in light condition was 69.3 ± 0.9 μW/m^2 when the LB-rGO thin film was treated at 100 W with Argon plasma (Figure 4.25). The result of power curves for both light and dark conditions indicates that significant contribution of power output was discovered during the dark condition for the 0W to 60W plasma treated LB-rGO thin films. This may occur due to the metabolism of organic substrates inside the algal cell secreted out during the absence of light (Fu et al., 2009; He et al., 2009). In addition, the sediment type of self-sustained phototropic microbial fuel cell has been reported to have improvement in electric current during dark condition while the current lessen in light condition (He et al., 2009). This phenomenon could be attributed to the unfavorable effect of oxygen production via photosynthesis process (He et al., 2009).

The power production in the dark condition may occur by the algal cell's ability to store its metabolite within itself. In photo-bioelectrochemical cells (Sekar et al., 2014), cynobacterium *Nostoc* sp. has been used on the anode as a photo-biocatalyst and current production in dark condition were reported to be low. This is possibly the results of the absence of the light in the linear photosynthetic pathway that drives the electron transport reaction (Ng et al., 2017). On the other hand, the result of the annealing treatment group of samples was quite surprising. It is because of the highest power density measured in light condition is 211.0 ± 1.0) μW/m^2 where the LB-rGO thin films have been treated at 400 ˚C temperature compared to the other various temperature treated samples. In comparison, the annealed LB-rGO thin films at 400 ˚C show a better result than LB-rGO thin films with Argon plasma treatment at 100 W. This situation may influenced by a low sheet resistivity value of 400 ˚C annealed LB-rGO thin films and its water contact angle compared to 100 W Argon plasma treated LB-rGO thin films (Figure 4.5 and Figure 4.6).

Besides, the improvement of BPV devices' power output are also related to the modification of anode surface apart from the other factors such as the chemical environment, solar radiation intensity, physical properties of electron acceptors and dissolved oxygen concentration (Pisciotta et al., 2010). According to recent research, the cellular behavior and interaction could possibly influenced by the surface topography of the cells including the roughness of the surface and the size of pores can be varied from micro to nanometers. In addition, the attachments of the *Chorella* sp. to the anode could be strengthen by the presence of the functional groups on the rGO sheets. Hence, improves its biocompatibility and produce higher power output (Ng et al., 2014c).

CHAPTER 5: CONCLUSIONS AND FUTURE RECOMMENDATION

5.1 Conclusions

All the objectives of this thesis were successfully achieved. The first objective involved deposition of LB-rGO thin films while the second was to optimize the rGO thin films by using LB technique and improve biocompatibility of the algae biofilms. Finally, the last objective involved conducting electrical characterization studies such as resistance measurements, power density and polarization curves on the fabricated LB-rGO thin films.

The experimental works carried-out shows the improvement in power density by using annealing treatment and Argon plasma treated LB-rGO thin films as the anode platform in BPV applications at particular value of parameters. For 100 W LB-rGO thin films, as shown in the wettability image Figure 4.8, the increase of hydrophilicity at 100 W LB-rGO thin films indicates the higher adhesiveness of the algae biofilm onto the rGO layer as well as improvement in its biocompatibility. On the other hand, the ratio I_D/I_G of LB-rGO thin film treated with Argon plasma (0.82) was observed to start to increase at 100 W (Table 4.3). This phenomenon indicates the existence of hydroxyl, epoxide and the other functional groups of oxygen as well. These functional groups effectively improved the hydrophilicity of LB-rGO thin film to facilitate biocompatibility to the algae biofilm. These results can be validated and supported by the results of maximum power density. As shown in Figure 4.25, the highest reading of maximum power density at light condition was observed at $(6.93 \pm 0.09) \times 10^{-5}$ W/m^2 representing the LB-rGO thin film treated with Argon plasma at 100 W. This was mainly attributed to the better adhesion achieved between the algae biofilms and the optimized surface of the rGO anode.

Meanwhile, for annealing treatment where LB-rGO thin film has been treated at 400 ˚C shows the lowest sheet resistivity (Figure 4.5) 3.47×10^4 Ω/sq. This result indicates in high conductivity of 400 ˚C LB-rGO thin film compared to other thin films that have been treated with different temperature. The value of conductivity shown by 400 ˚C LB-rGO thin film is significant in assisting the harvested electron travel to the electrode. 400 ˚C LB-rGO thin film is a great candidate for electrode in BPV due to its conductivity and also possess biocompatible ability. This can be supported by the results of contact angle where it has the lowest value 86.45˚, hence indicates an increment in hydrophilicity. Moreover, the optimum reading of maximum power density at light condition was observed at $(2.11 \pm 0.01) \times 10^{-4}$ W/m^2 representing the LB-rGO thin film treated with 400 ˚C.

5.2 Future Recommendation

The development of treated LB-rGO thin films as reported in this work highlights the potential of green technology applications as a result of the optimization process. In addition, further studies in relation between the algae and the anode platform will help in better understanding their interactions in order to improve the device efficiency. In this work, the treated LB-rGO thin films help in improving the BPV device performance by altering its surface morphology. The outcome of this work will have a positive impact towards enhancing the performance of BPV devices and other similar applications in future.

REFERENCES

An, S., Zhu, Y., Lee, S., Stoller, M., Emilsson, T., & Park, S. et al. (2010). Thin Film Fabrication and Simultaneous Anodic Reduction of Deposited Graphene Oxide Platelets by Electrophoretic Deposition. *The Journal of Physical Chemistry Letters*, *1*(8), 1259-1263.

Angioni, S., Millia, L., Mustarelli, P., Doria, E., Temporiti, M., & Mannucci, B., …Quartarone, E. (2018). Photosynthetic microbial fuel cell with polybenzimidazole membrane: synergy between bacteria and algae for wastewater removal and biorefinery. *Heliyon*, *4*(3), Article #e00560.

Badura, A., Esper, B., Ataka, K., Grunwald, C., Wöll, C., Kuhlmann, J., …Rögner M. (2006). Light-driven water splitting for (bio-)hydrogen production: Photosystem 2 as the central part of a bioelectrochemical device. *Photochemistry and Photobiology*, *82*(5), 1385-1390.

Blankenship, R., & Hartman, H. (1998). The origin and evolution of oxygenic photosynthesis. *Trends in Biochemical Sciences*, *23*(3), 94-97.

Blodgett, K. (1935). Films built by depositing successive monomolecular layers on a solid surface. *Journal of The American Chemical Society*, *57*(6), 1007-1022.

Bombelli, P., Bradley, R., Scott, A., Philips, A., McCormick, A., Cruz, S., …Fisher, A. (2011). Quantitative analysis of the factors limiting solar power transduction by *Synechocystis sp. PCC 6803* in biological photovoltaic devices. *Energy & Environmental Science*, *4*(11), 4690-4698.

Bombelli, P., McCormick, A., Bradley, R., Yunus, K., Philips, J., Anderson X., … Fisher, A. (2011) Harnessing solar energy by bio-photovoltaic (BPV) devices. *Communications in Agricultural and Applied Biological Sciences, 76*(2), 89-91.

Bombelli, P., Müller, T., Herling, T., Howe, C., & Knowles, T. (2014). A high power-density, mediator-free, microfluidic biophotovoltaic device for cyanobacterial cells. *Advanced Energy Materials*, *5*(2), Article #1401299.

Brennan, L., & Owende, P. (2010). Biofuels from microalgae—A review of technologies for production, processing, and extractions of biofuels and co-products. *Renewable and Sustainable Energy Reviews*, *14*(2), 557-577.

Brown, R., Larson, D., & Bold, H. (1964). Airborne Algae: Their Abundance and Heterogeneity. *Science*, *143*(3606), 583-585.

Campbell, M. (2008). Biodiesel: algae as a renewable source for liquid fuel. *Guelph Engineering Journal, 2*(1), 2-7.

Cassie, A., & Baxter, S. (1944). Wettability of porous surfaces. *Transactions of The Faraday Society*, *40*, 546-551.

Chen, D., Feng, H., & Li, J. (2012). Graphene oxide: Preparation, functionalization, and electrochemical applications. *Chemical Reviews.*, *112*(11), 6027-6053.

Chisti, Y. (2007). Biodiesel from microalgae. *Biotechnology Advances*, *25*(3), 294-306.

Choi, W., Lahiri, I., Seelaboyina, R., & Kang, Y. S. (2010). Synthesis of graphene and its applications: A Review. *Critical Reviews in Solid State and Materials Sciences, 35*(1), 52-71.

Chung, C., Kim, Y. K., Shin, D., Ryoo, S. R., Hong, B. H., & Min, D. H. (2013). Biomedical applications of graphene and graphene oxide. *Accounts of Chemical Research*, *46*(10), 2211-2224.

Crewe, A. (1983). High-resolution scanning transmission electron microscopy. *Science*, *221*(4608), 325-330.

C. Gray, J. (2011). Understanding Photosynthesis: How Does Chlorophyll Absorb Light Energy?. Retrieved on 26th July 2018 from http://www.saps.org.uk

Cote, L., Kim, J., Zhang, Z., Sun, C., & Huang, J. (2010). Tunable assembly of graphene oxide surfactant sheets: Wrinkles, overlaps and impacts on thin film properties. *Soft Matter*, *6*(24), 6096-6101.

Das, K., Sah, B., & Kundu, S. (2017). Cation-induced monolayer collapse at lower surface pressure follows specific headgroup percolation. *Physical Review E*, *95*(2) Article #022804.

Demirbas, A., & Fatih Demirbas, M. (2011). Importance of algae oil as a source of biodiesel. *Energy Conversion And Management*, *52*(1), 163-170.

Eda, G., Fanchini, G., & Chhowalla, M. (2008). Large-area ultrathin films of reduced graphene oxide as a transparent and flexible electronic material. *Nature Nanotechnology*, *3*(5), 270-274.

Fenn, M., Xanthopoulos, P., Pyrgiotakis, G., Grobmyer, S., Pardalos, P., & Hench, L. (2011). Raman spectroscopy for clinical oncology. *Advances in Optical Technologies*, *2011*, 1-20.

Fu, C., Su, C., Hung, T., Hsieh, C., Suryani, D., & Wu, W. (2009). Effects of biomass weight and light intensity on the performance of photosynthetic microbial fuel cells with Spirulina platensis. *Bioresource Technology*, *100*(18), 4183-4186.

Gao, Y., Yip, H., Chen, K., O'Malley, K., Acton, O., Sun, Y., …Jen, A. K. Y. (2011). Surface doping of conjugated polymers by graphene oxide and its application for organic electronic devices. *Advanced Materials*, *23*(16), 1903-1908.

Girard-Egrot, A., & Blum, L. (2007). Langmuir-Blodgett technique for synthesis of biomimetic lipid membranes. *Nanobiotechnology of Biomimetic Membranes*, 23-74.

Giusfredi, G., Bartalini, S., Borri, S., Cancio, P., Galli, I., Mazzotti, D., & De Natale, P. (2010). Saturated-Absorption Cavity Ring-Down Spectroscopy. *Physical Review Letters*, *104*(11).

Gouveia, L., & Oliveira, A. (2008). Microalgae as a raw material for biofuels production. *Journal of Industrial Microbiology & Biotechnology*, 36(2), 269-274.

Gude, V., Kokabian, B., & Gadhamshetty, V. (2013). Beneficial bioelectrochemical systems for energy, water, and biomass production. *Journal of Microbial & Biochemical Technology*.

Guo, D., Xie, G., & Luo, J. (2013). Mechanical properties of nanoparticles: Basics and applications. *Journal of Physics D: Applied Physics*, *47*(1), Article #013001.

Gupta, R., & Manjuladevi, V. (2012). Molecular interactions at interfaces. In Aurelia A. Meghea, *Molecular interactions* (1st ed.). *IntechOpen*. Retrieved on 3rd March 2017 from https://www.intechopen.com

He, Z., Kan, J., Mansfeld, F., Angenent, L., & Nealson, K. (2009). Self-sustained phototrophic microbial fuel cells based on the synergistic cooperation between photosynthetic microorganisms and heterotrophic bacteria. *Environmental Science & Technology*, *43*(5), 1648-1654.

Huang, X., Qi, X., Boey, F., Zhang, H. (2012). Graphene-based Composites. *Chemical Society Reviews, 41*(2), 666-686.

Huang, M., Biswal, M., Park, H., Jin, S., Qu, D., & Hong, S., …Rouff, R. (2018). Highly oriented monolayer graphene grown on a Cu/Ni(111) alloy foil. *ACS Nano*, *12*(6), 6117-6127.

Hwang, J., Amy, F., & Kahn, A. (2006). Spectroscopic study on sputtered PEDOT·PSS: Role of surface PSS layer. *Organic Electronics*, *7*(5), 387-396.

Jaafar, M., Ciniciato, G., Ibrahim, S., Phang, S., Yunus, K., Fisher, A., …Periasamy, V. (2015). Preparation of a three-dimensional reduced graphene oxide film by using the Langmuir–Blodgett method. *Langmuir*, *31*(38), 10426-10434.

Jalvandi. J. (2016). *Novel chemical and physical approaches for sustainable drug release from biodegradable electrospun nanofibres*. (Doctoral dissertation). Retrieved on 4th September 2018 from https://www.researchgate.net

Janzen, A., & Seibert, M. (1980). Photoelectrochemical conversion using reaction-centre electrodes. *Nature*, *286*(5773), 584-585.

Kalinowski, J. (1999). Electroluminescence in organics. *Journal of Physics D: Applied Physics*, *32*(24), R179-R250.

Kavitha, M. K., John, H., Gopinath, P., & Philip, R. (2013). Synthesis of reduced graphene oxide–ZnO hybrid with enhanced optical limiting properties. *Journal of Materials Chemistry C, 1*(23), 3669-3676.

Kim, H., Mattevi, C., Kim, H., Mittal, A., Mkhoyan, K., Riman, R., & Chhowalla, M. (2013). Optoelectronic properties of graphene thin films deposited by a Langmuir–Blodgett assembly. *Nanoscale*, *5*(24), 12365-12374.

Kuhn, H., & Möbius, D. (1971). Systems of monomolecular layers-assembling and physico-chemical behavior. *Angewandte Chemie International Edition in English*, *10*(9), 620-637.

Kumar, P., Bernardi, M., & Grossman, J. (2013). The impact of functionalization on the stability, work function, and photoluminescence of reduced graphene oxide. *ACS Nano*, 7(2), 1638-1645.

Lam, K., Johnson, E., Chiao, M., & Lin, L. (2006). A MEMS photosynthetic electrochemical cell powered by subcellular plant photosystems. *Journal of Microelectromechanical Systems*, *15*(5), 1243-1250.

Langmuir Films - Nanoscience Instruments. (2019). Retrieved on 8th February 2018 from https://www.nanoscience.com

Law, K. (2014). Definitions for hydrophilicity, hydrophobicity, and superhydrophobicity: Getting the basics right. *The Journal of Physical Chemistry Letters*, 5(4), 686-688.

Lee, D., Chang, J., & Lai, J. (2015). Microalgae–microbial fuel cell: A mini review. *Bioresource Technology*, *198*, 891-895.

Lee, R. (2008). *Phycology (4th ed.,* pp. *3-4)*. New York: Cambridge University Press.

Li, X., Zhang, G., Bai, X., Sun, X., Wang, X., Wang, E., & Dai, H. (2008). Highly conducting graphene sheets and Langmuir–Blodgett films. *Nature Nanotech*, *3*(9), 538-542.

Lightcap, I.; Kamat, P. V. (2013). Graphitic design: Prospects of graphene-based nanocomposites for solar energy conversion, storage, and sensing. *Accounts of Chemical Research, 46*(10), 2235-2243.

Logan, B., Hamelers, B., Rozendal, R., Schröder, U., Keller, J., Freguia, S., …Rabaey, K. (2006). Microbial fuel cells: Methodology and technology. *Environmental Science & Technology*, *40*(17), 5181-5192.

Loryuenyong, V., Totepvimarn, K., Eimburanapravat, P., Boonchompoo, W., & Buasri, A. (2013). Preparation and characterization of reduced graphene oxide sheets via water-based exfoliation and reduction methods. *Advances in Materials Science and Engineering*, Article #923403.

Malik, S., Drott, E., Grisdela, P., Lee, J., Lee, C., & Lowy, D. (2009). A self-assembling self-repairing microbial photoelectrochemical solar cell. *Energy & Environmental Science*, 2(3), 292-298.

Maly, J., Masojidek, J., Masci, A., Ilie, M., Cianci, E., Foglietti, V., …Pilloton, R. (2005). Direct mediatorless electron transport between the monolayer of photosystem II and poly(mercapto-p-benzoquinone) modified gold electrode—new design of biosensor for herbicide detection. *Biosensors and Bioelectronics*, *21*(6), 923-932.

Mathuriya, A. (2014). Eco-affectionate face of microbial fuel cells. *Critical Reviews In Environmental Science and Technology*, *44*(2), 97-153.

Mattevi, C., Eda, G., Agnoli, S., Miller, S., Mkhoyan, K., & Celik, O. (2009). Evolution of electrical, chemical, and structural properties of transparent and conducting chemically derived graphene thin films. *Advanced Functional Materials*, *19*(16), 2577-2583.

McCormick, A., Bombelli, P., Scott, A., Philips, A., Smith, A., Fisher, A., & Howe, C. (2011). Photosynthetic biofilms in pure culture harness solar energy in a mediatorless bio-photovoltaic cell (BPV) system. *Energy & Environmental Science*, *4*(11), 4699-4709.

Milledge, J., Smith, B., Dyer, P., & Harvey, P. (2014). Macroalgae-derived biofuel: A review of methods of energy extraction from seaweed biomass. *Energies*, *7*(11), 7194-7222.

Moazzami Gudarzi, M. (2012). Enhancement of dispersion and bonding of graphene-polymer through wet transfer of functionalized graphene oxide. *Expresspolymlett*, *6*(12), 1017-1031.

Morançais, M., Mouget, J., & Dumay, J. (2018). Proteins and Pigments. In I. A. Levine & J. Fleurence, *Microalgae in Health and Disease Prevention 2018,* (pp. 145-175). Academic Press.

Najafpour, G., Rahimnejad, M., & Ghoreshi, A. (2011). The enhancement of a microbial fuel cell for electrical output using mediators and oxidizing agents. *Energy Sources, Part A: Recovery, Utilization, And Environmental Effects*, *33*(24), 2239-2248.

Ng, F., Phang, S., Periasamy, V., Yunus, K., & Fisher, A. (2014a). Algae biofilm on indium tin oxide electrode for use in biophotovoltaic platforms. *Advanced Materials Research*, *895*, 116-121.

Ng, F., Phang, S., Periasamy, V., Yunus, K., & Fisher, A. (2014b). Evaluation of Algal Biofilms on Indium Tin Oxide (ITO) for Use in Biophotovoltaic Platforms Based on Photosynthetic Performance. *Plos ONE*, *9*(5), Article #e97643.

Ng, F., Jaafar, M., Phang, S., Chan, Z., Salleh, N., Azmi, S., …Periasamy, V. (2014c). Reduced graphene oxide anodes for potential application in algae biophotovoltaic platforms. *Scientific Report*, *4*(7562), 1-7.

Ng, F., Phang, S., Periasamy, V., Yunus, K., & Fisher, A. (2017). Enhancement of Power Output by using Alginate Immobilized Algae in Biophotovoltaic Devices. *Scientific Reports*, *7*(1), Article #16237.

Ng, F., Phang, S., Periasamy, V., Beardall, J., Yunus, K., & Fisher, A. (2018). Algal biophotovoltaic (BPV) device for generation of bioelectricity using Synechococcus elongatus (Cyanophyta). *Journal of Applied Phycology*, *30*(6), 2981-2988.

Niinivaara, E., Wilson, B., King, A., & Kontturi, E. (2016). Parameters affecting monolayer organisation of substituted polysaccharides on solid substrates upon Langmuir–Schaefer deposition. *Reactive and Functional Polymers*, *99*, 100-106.

Novoselov, K. (2004). Electric field effect in atomically thin carbon films. *Science*, *306*(5696), 666-669.

Ozkan, A., & Berberoglu, H. (2013). Adhesion of algal cells to surfaces. *Biofouling*, *29*(4), 469-482.

Pandit, S., & Das, D. (2015). Role of microalgae in microbial fuel cell. *Algal Biorefinery: An Integrated Approach*, *1*(17), 375-399.

Paredes, J., Villar-Rodil, S., Martínez-Alonso, A., & Tascón, J. (2008). Graphene oxide dispersions in organic solvents. *Langmuir*, *24*(19), 10560-10564.

Park, S. & Ruoff, R. (2009). Chemical methods for the production of graphenes. *Nature Nanotech*, *4*(4), 217-224.

Patil, V., Reitan, K. I., Knudsen, G., Mortensen, L., Kallqvist, T., Olsen, E., …Gislerod, H. (2005) Microalgae as source of polyunsaturated fatty acids for aquaculture. *Research Trends*, (6), 57–65.

Paul, S., Pearson, C., Molloy, A., Cousins, M., Green, M., Kolliopoulou, S., …Petty, M. C. (2003). Langmuir−Blodgett film deposition of metallic nanoparticles and their application to electronic memory structures. *Nano Letters*, *3*(4), 533-536.

Pham, V. H., Cuong, T. V., Hur, S. H., Oh, E., Kim, E. J., Shin, E. W., & Chung, J. S. (2011). Chemical functionalization of graphene sheets by solvothermal reduction of a graphene oxide suspension in N-methyl-2-pyrrolidone. *Journal of Material Chemistry, 21*(10), 3371-3377.

Phang SM, Chu WL (1999). Catalogue of Strains, University of Malaya Algae Culture Collection (UMACC). Institute of Postgraduate Studies and Research, University of Malaya, Kuala Lumpur.

Pisciotta, J., Zou, Y., & Baskakov, I. (2010). Light-dependent electrogenic activity of cyanobacteria. *Plos ONE*, 5(5), Article #e10821.

Pumera, M. (2010). Graphene-based nanomaterials and their electrochemistry. *Chemical Society Reviews*, *39*(11), 4146-4157.

Rabaey, K., & Verstraete, W. (2005). Microbial fuel cells: Novel Biotechnology for Energy Generation. *Trends In Biotechnology*, *23*(6), 291-298.

Rahimnejad, M., Adhami, A., Darvari, S., Zirepour, A., & Oh, S. (2015). Microbial fuel cell as new technology for bioelectricity generation: A review. *Alexandria Engineering Journal*, *54*(3), 745-756.

Rasuli, R., Iraji zad, A., & Ahadian, M. (2010). Mechanical properties of graphene cantilever from atomic force microscopy and density functional theory. *Nanotechnology*, *21*(18), Article #185503.

Rayleigh. (1891). Surface Tension. *Nature*, *43*(1115), 437-439.

Sekar, N., Umasankar, Y., & Ramasamy, R. (2014). Photocurrent generation by immobilized cyanobacteria via direct electron transport in photo-bioelectrochemical cells. *Physical Chemistry Chemical Physics*, *16*(17), 7862-7871.

Sygellou, L., Paterakis, G., Galiotis, C., & Tasis, D. (2015). Work function tuning of reduced graphene oxide thin films. *The Journal of Physical Chemistry C*, *120*(1), 281-290.

Tan, L., Ong, W., Chai, S., & Mohamed, A. (2013). Reduced graphene oxide-TiO_2 nanocomposite as a promising visible-light-active photocatalyst for the conversion of carbon dioxide. *Nanoscale Research Letters*, *8*(934), 465-480.

Tschörtner, J., Lai, B., & Krömer, J. (2019). Biophotovoltaics: Green power generation from sunlight and water. *Frontiers in Microbiology*, *10*(866), 1-5.

Van Le, Q., Choi, J., & Kim, S. (2017). Recent advances in the application of two-dimensional materials as charge transport layers in organic and perovskite solar cells. *Flatchem*, 2, 54-66.

Yang, Y., Sun, G., & Xu, M. (2011). Microbial fuel cells come of age. *Journal of Chemical Technology & Biotechnology*, *86*(5), 625-632.

Yang, Y., Yang, X., Yang, W., Li, S., Xu, J., & Jiang, Y. (2014). Ordered and ultrathin reduced graphene oxide LB films as hole injection layers for organic light-emitting diode. *Nanoscale Research Letters*, *9*(1), 537-543.

Yin, Z., Sun, S., Salim, T., Wu, S., Huang, X., He, Q., …Zhang, H. (2010). Organic Photovoltaic Devices Using Highly Flexible Reduced Graphene Oxide Films as Transparent Electrodes. *ACS Nano*, *4*(9), 5263-5268.

Zbik, M. (1998). Nanomorphology of Kaolinites: Comparative SEM and AFM Studies. *Clays and Clay Minerals*, *46*(2), 153-160.

Zhong, Z., Wu, W., Wang, D., Wang, D., Shan, J., Qing, Y., & Zhang, Z. (2010). Nanogold-enwrapped graphene nanocomposites as trace labels for sensitivity enhancement of electrochemical immunosensors in clinical immunoassays: Carcinoembryonic antigen as a model. *Biosensors and Bioelectronics, 25*(10), 2379-2383.

Zhou, G., Wang, D., Li, F., Zhang, L., Li, N., Wu, Z., …Cheng, H. (2010). Graphene-wrapped Fe_3O_4 anode material with improved reversible capacity and cyclic stability for lithium ion batteries. *Chemistry of Materials, 22*(18), 5306-5313.

Zhu, Y., Murali, S., Cai, W., Li, X., Suk, J., Potts, J., & Ruoff, R. (2010). ChemInform abstract: Graphene and graphene oxide: synthesis, properties, and applications. *Cheminform, 41*(45), 3906-3924.

Zhu, X., Zhu, Y., Murali, S., Stoller, M., & Ruoff, R. (2011). Nanostructured reduced graphene oxide/Fe_2O_3 composite as a high-performance anode material for lithium ion batteries. *ACS Nano, 5*(4), 3333-3338.

LIST OF PUBLICATION AND PAPER PRESENTED

List of Publication

1. **Ibrahim, S.**, Jaafar, M., Ng, F., S.M. Phang, Kumar, G., Majid, W., & Periasamy, V. (2017). Plasma-treated Langmuir–Blodgett reduced graphene oxide thin film for applications in biophotovoltaics. *Applied Physics A*, *124*(1), 59-63.

Paper Presented

1. **Ibrahim, S.**, Jaafar, M., Ng, F., S.M. Phang, Majid, W., & Periasamy, V. (2016). *Characterization of annealing temperature and plasma treatment for surface functionalization of reduced graphene oxide anodic films for biophotovoltaic applications*. Paper presented at the 2nd International Science, Technology, and Engineering Conference (ISTEC), 20 – 23 April 2016, Penang, Malaysia.